SHORT GLASS FIBER REINFORCED COMPOSITES MANUFACTURED BY STEREOLITHOGRAPHY

A Thesis
Submitted to the Graduate Faculty
of the
North Dakota State University
of Agriculture and Applied Science

By

Michael John Holthaus

In Partial Fulfillment of Requirements
for the Degree of
MASTER OF SCIENCE

Major Department:
Mechanical Engineering

November 2020

Fargo, North Dakota

North Dakota State University

Graduate School

Title

SHORT GLASS FIBER REINFORCED COMPOSITES MANUFACTURED BY STEREOLITHOGRAPHY

By

Michael John Holthaus

The Supervisory Committee certifies that this ***disquisition*** complies with North Dakota State University's regulations and meets the accepted standards for the degree of

MASTER OF SCIENCE

SUPERVISORY COMMITTEE:

Dr. Chad Ulven

Chair

Dr. Dean Webster

Dr. Long Jiang

Approved:

01/19/2021

Date

Dr. Alan Kallmeyer

Department Chair

ABSTRACT

The effectiveness of manufacturing short glass fiber composites using stereolithography (SLA) was investigated. Modifications were made to a standard SLA printer to induce a flow field through the resin tank. In this study a 1/32 inch glass fiber content of 15% by volume was printed in combination with a commercial Peopoly SLA UV curable resin. Testing was performed for fiber dispersion and whether the addition of glass fiber would increase the mechanical properties of the composites. While printing it was found the surface finish of the specimens was coarse from the glass fibers. Computational fluid dynamics simulations were performed to observe flow around the printed parts. The results of the tests concluded the glass fiber increased some properties but had negligible effects on others. Further investigation involving various fibers and different sizing of the fibers have the potential to increase the mechanical properties found in the research.

ACKNOWLEDGEMENTS

I would like to thank the Army Research Laboratory for the opportunity to investigate SLA printers and fiber composites. I would also like to thank Dr. Chad Ulven for suggesting this research and guiding me in this journey. Additionally, I would like to thank Luke Gibbon for is direction and editing skills, I would like to thank Bailey Carlson for helping design the CFD simulations, and I would like to the thank the NSF for allowing me to use the scanning electron microscope. Lastly, I would like to thank my committee members, Dr. Dean Webster and Dr. Long Jiang.

TABLE OF CONTENTS

LIST OF TABLES

LIST OF FIGURES

LIST OF APPENDIX FIGURES

1. INTRODUCTION

1.1. Additive Manufacturing

Through additive manufacturing (AM), a faster production of prototypes and other small objects can be achieved. The ability to customize any object quickly provides a new advantage to companies, designers, and hobbyists to optimize manufacturing needs. With AM, objects are created layer by layer. These techniques are controlled by computer software that allows the user to manipulate the different printer settings.

AM begins by making a 3D model of the object, this can be done using a number of different 3D modelling software. To allow for the part to be manufactured successfully the part file must be changed from a native file to neutral file to be recognized by other software. In these formats, the object is broken down into a 3D mesh. Depending on which AM type machine is being used another software such as Asura or Cura must be used to create a tool path called a G-code. The G-code controls all aspects of the printer, including the X and Y direction of the laser, the Z direction of the print bed, layer height, the speed of the laser, and if needed sweep step or peel step.

1.2. Advantages and Disadvantages of AM

Over the past two decades AM has become a widely used method to create objects from all material types (i.e., metals, ceramics, and polymers). Additive manufacturing continues to improve with advancements in technologies. Now companies can produce fully functional parts that can be sold to the public rather than being used strictly for prototyping purposes. Although there have been great strides to improve these technologies, they still present some limitations.

1.2.1. Advantages

The first advantage discovered was the ability to have complete customization of part design. The limitations of small corners or difficult geometries were greatly reduced and the need for tooling to produce the object was eliminated. This was because the objects being manufactured are created from a single layer from the base of the object to the last layer at the top. It was now possible to make hidden shapes inside larger shapes eliminating space for tool heads. Objects are printed in one solid piece and do not require joining concepts like adhesive, bolts, or nails. Joints can be a sources of stress concentration and ultimately lead to part failure, increase cost and, increase the total weight of the part being manufactured. Eliminating joints also can reduce the time needed for an employee to assemble the object, thereby lowering the total cost of each object. The only overhead cost of the piece being manufactured is the printer and the resin/filament. Before AM, prototyping could be a costly and time-consuming endeavor. With the advancements in AM technology, new ideas for a product can be made in a matter of hours instead of days or weeks.

1.2.2. Disadvantages

One of the disadvantages of AM is the lower mechanical performance of printed parts as compared to the same materials manufactured in a subtractive manner. There are a few reasons for these performance shortcomings. First, there can be poor layer-to-layer adhesion in the printed parts when each layer is independently placed on top of the next. This means the interface between the layers can break away from each other at a lower stress than that required to fracture the bulk material. Another reason is that compared to subtractive manufacturing, AM is more limited in the number of materials that can be used. Another disadvantage is that AM can require high capital costs. The printers typically required are expensive and the materials used to

print can also have a high cost due the powder form they need to be in and how they need to be handled as a result.

1.3. 3D Printing

A term commonly used for polymer AM approaches is called 3D printing. Different forms of polymer 3D printing have been available for over three decades [1]. For the purpose of this thesis, only fused deposition modeling (FDM), stereolithography (SLA), and digital light synthesis (DLS) will be discussed. These printing processes use polymers, for example, FDM uses thermoplastic such as acrylonitrile butadiene styrene (ABS) and poly(lactic acid) (PLA) [2]. On the other hand, SLA and DLS use a liquid thermoset. The most popular resin used in SLA printer are acrylate based and take advantage monomers and photo polymerization initiators to cure [3] which will be explained later in the thesis.

FDM printing uses a long filament of thermoplastic pushed through a heated nozzle and melts. The melted filament is then laid onto a heated bed. The thermoplastic filament then cools and solidifies, as this happens, the thermoplastic polymer begins to shrink. The size of each layer is dependent on the user and how the print is to be made [4]. This can be seen in Figure 1 below.

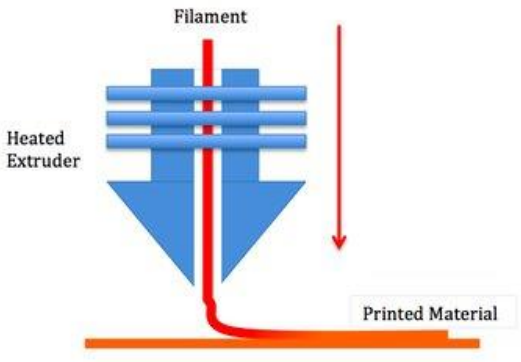

Figure 1: Diagram of an FDM printer nozzle [1].

Stereolithography printers manufacture objects by curing a photopolymer liquid resin into a solid object. During the SLA process a laser path is accomplished by using a computer guided

light source, the light source used in these experiments is an UV laser, the resin used is an acrylate functionalized monomer that is polymerized by free radical polymerization. This is similar to DLS but, instead of a laser path it is a projected image on the build plate. The free radicals in the resin are photoinitiated by the UV laser or UV projected image. The laser used must be in the wavelength range of the free radicals or, the resin will not cure properly also, the diameter of the laser must be in the range of the free radicals along with the wavelength [5]. A traditional SLA printer can be seen below in Figure 2.

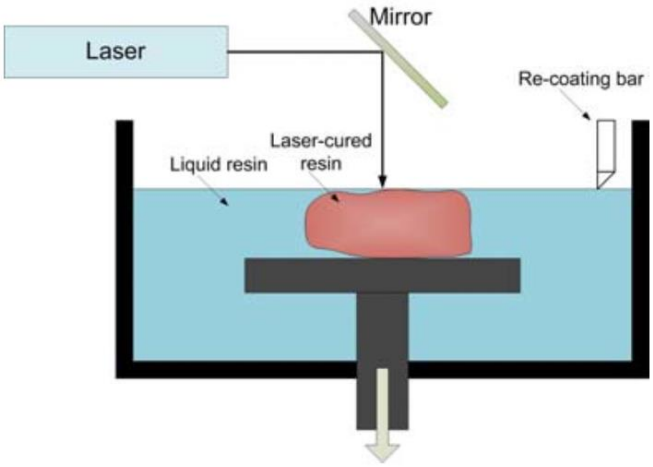

Figure 2: Diagram of a traditional SLA printer setup [6].

Many researchers have been looking for new ways to improve the quality of polymer 3D printing over the past several decades. Polymer chemists have considered chemistry-based approaches to change the base elements of the resin being used [7], as engineers have tried adding different fibers to the resin to improve the printed part's mechanical properties [8]. The addition of fibers to the resin is a new field with much potential of increasing mechanical properties. The research discussed in this thesis will explain how glass fiber reinforcement will improve the mechanical properties in test samples and describe implications that come with altering a tried system.

1.4. SLA Printers

Different objects have been printed using SLA printers since the mid 1970's when a Japanese researcher named Dr. Hideo Kodama discovered how to turn a UV curable resin into a solid object. In this first technology, Dr. Kodama [9] used a photosensitive polymer and UV light to cure the polymer. This is an example of the first use, but the patented process seen today was described by Charles W. Hull. He was also the first person to coin the term stereolithography. He would later go on to patent the term and process known today. The term "printing" means to add a layer on top of an already existing layer and make a 3D object [9]. It was not until the mid-2000s that SLA printers became widely used. The reason for this is that it took 20 years for the first patent to expire. Now there are numerous companies producing their own SLA type of printers and resins.

There are four regularly used types of SLA printers that use liquid resin. The first is a traditional SLA top down approach, the second is an inverted SLA approach, and the third is a combination of both technologies. The fourth, is DLS and has a similar setup as inverted but has a projector instead of a laser.

The traditional SLA printer operates by using the laser on top of the print bed. The laser will print layer by layer in a tank of liquid resin, after each pass of the laser, a recoating blade will cross over the printed object to ensure that a new coating of resin is placed on top of the part. The print bed lowers after each pass to create the object from the bottom up. An advantage of this type of printer is there is no peel step, this will be discussed later in the inverted SLA printing process. One drawback of the traditional SLA printer is the large amount of resin needed to fill the tank. A solution to this was to make printers with smaller tanks, but this limits the size

of the parts. Another drawback of the traditional SLA printer is it is more expensive than an inverted SLA printer [9]. An inverted approach can be seen in Figure 3 below.

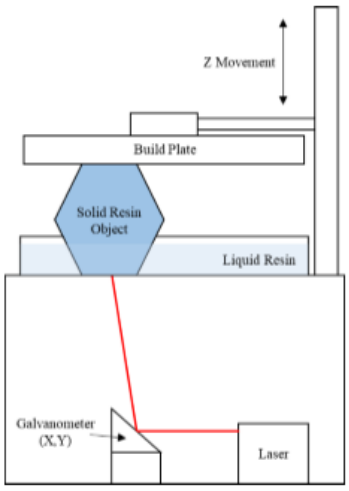

Figure 3: Diagram of an inverted SLA printer setup [6].

The inverted approach has different steps that are needed to ensure a successful print. Opposite of the traditional approach, a laser points up from the bottom of the printer bed and the build plate moves up in the Z axis instead of down. The resin tank is much smaller than the traditional approach. Additionally, instead of a wipe step there is a peel step. This peel step is used after every layer is printed. During the peel step of the inverted process, the resin tank will pivot on the X axis to allow for resin to flow underneath the recently printed layer. As this happens problems can occur, if the object being printed is not properly attached to the build plate it will cause stresses on the object being printed. If this happens, there is a potential for the printed object to break free from the build plate. There are settings in some printers such as the one used in this research that allow for this peel step to be manipulated to be either faster or slower depending on what shape of object is being manufactured.

The third type of regularly used printing types is a combination of traditional and inverted. This printing type resembles an inverted printer but does not have the peel step to move

the resin. Instead, there is blade that will sweep back and forth in similar fashion to that of a traditional printer. The advantages of not having a peel step is there will be no unneeded stress put on the printed part. The bed of the tank is also made from a different kind of silicone base layer in order to reduce sticking to the tank bed.

The fourth type is from a company called Carbon 3D. Instead of using a laser, Carbon 3D has developed a process called Digital Light Synthesis (DLS) which use a projector. The DLS process and setup is identical to that of the inverted SLA process, the only change is where the laser would be for SLA a light projector is place. The advantage of this process is the speed at which parts can be manufactured. DLS use an oxygen permeable window that allows for a unique area called the dead zone. In this area a small amount of liquid resin is in between the solid part and the window. As the light hits the resin it cures to the solid part, but not in the area near the oxygen permeable window eliminating a need of a peel step like inverted SLA. After the part is printed it is then placed in an oven producing a final cure. Once fully cured the final part exhibit a Young's modulus as high as 4000 MPa. This new form of 3D printing also allows for a more predictable and consistent mechanical properties [10].

Manufacturing with a 3D printer has many advantages, such as speed and total customization. Both these factors have made 3D printing successful. The largest drawback comes with the overall strength of the finished part, increased mechanical properties will allow for a larger range application for 3D printing. The purpose of this research is to find a new way to improve the mechanical properties of these parts. By introducing the fibers to the matrix, it will allow the fibers to take the majority of the force, instead of the low strength/ low modulus characteristics of UV resin. Improving the mechanical properties of the finished part will not

only help 3D printer hobbyist but could be used for military or medical research and manufacturing.

2. BACKGROUND

2.1. Fiber Reinforcement

SLA printers are not a new form of AM but adding reinforcement has been researched by far fewer people. Carbon fiber is one of the strongest reinforcements that can be combined with a polymer matrix, which would render higher properties such as Young's modulus and tensile strength. The concept of this was previously researched by Patrick Simpson [6]. Simpson [6] was able to add 5% by weight of carbon fibers to a UV resin matrix. It was found that adding carbon fiber had the potential to increase the final strength of the prints, but it came with drawbacks. The major problem was the carbon fibers are opaque to UV light. Because UV light is not able to pass through the carbon fiber the UV resin could not fully cure.

In Simpson's [6] research, a thermal initiator was added to the resin in order to produce a final cure. While adding the thermal initiator solved the problem of optimally curing the part it also created voids in the printed samples, which happens when the thermal initiator gives off small amounts of nitrogen gas as it heats [6]. The gas then gets trapped creating small voids [11]. A Scanning Electron Microscope (SEM) was used to find void content and it was later explained that the voids were reducing the potential high strength of the parts being manufactured as each of these voids acted as a stress concentration point [6].

Incorporation of glass fibers have also been investigated by engineers to increase the mechanical properties in AM. In a recent study, it was found that it was possible to print with a fiber volume of 50% by weight of powdered glass, the study also examined printing short glass fiber at a length of 15 mm mixed with a UV curable resin. The fibers and resin were mixed in a planetary mixer for 10 min at 80 rpm [12].

The results of the study showed that adding the glass fiber increased the overall mechanical properties of the UV curable resin but, the overall quality of the print diminished as percent volume of fibers increased. The results of tensile tests can be seen in Figure 4.

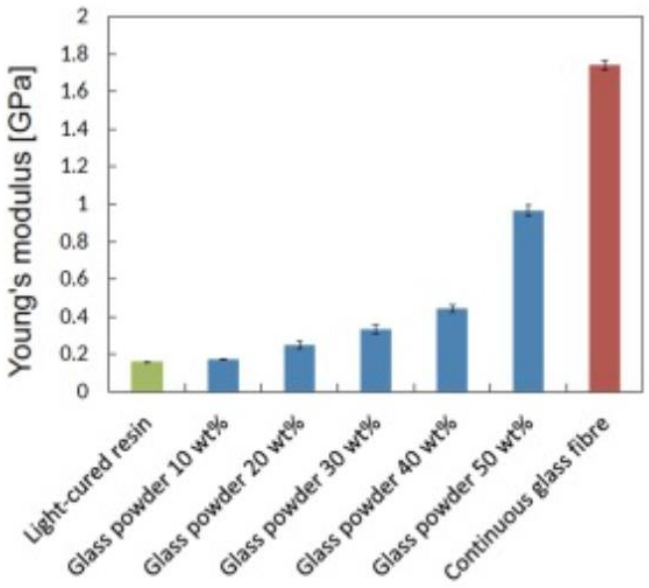

Figure 4: Young's modulus of different fiber volume fractions [12].

The researchers were able to conclude that the presence of glass fiber increased the Young's modulus of the composite as well as increase the tensile strength. The graph of this can be seen below in Figure 5.

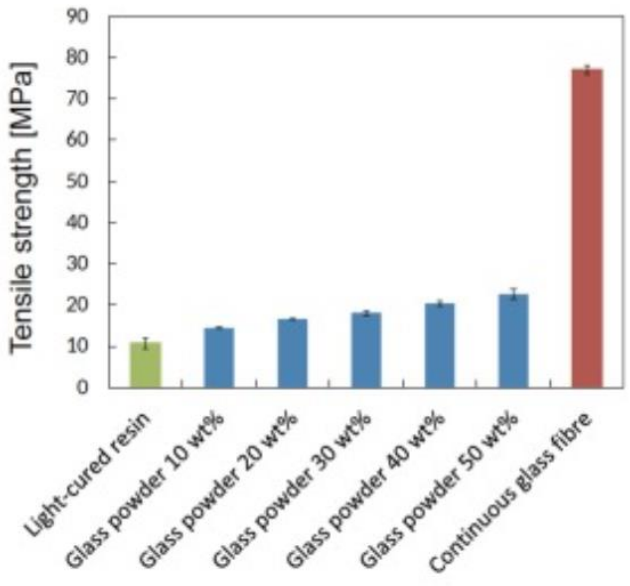

Figure 5: Tensile strength at different fiber volumes [12].

The addition of glass powder was able to increase both the Young's modulus and the tensile strength of the composite. It is also worth noting that the researchers had concerns over the dispersion of fiber among the prints, the researcher also stated the beginning section of the print had a darker color indicating a larger fiber fraction than that of remaining section of the print [12].

Similar to the SLA process, thermoplastics used in FDM exhibit low mechanical properties without reinforcement. MarkForged manufactures an FDM printer filament that incorporates continuous carbon fiber in a thermoplastic. Researchers have been comparing this process and evaluating the advantages of using carbon-fiber in thermoplastics filament. Two different thermoplastics were used (ABS) and (PLA) in a recent study done by L.G. Blok, M.L. Longana, H. Yu, and B.K.S Woods [13]. The researchers wanted to find the benefits of the carbon fiber reinforced thermoplastic. As expected, the mechanical properties of tensile strength, Young's modulus, fracture toughness etc. were improved. Further examining the prints, some disadvantages arose. When the force was applied in the transverse direction of the fiber, no gain

in properties was found, a small decrease in the properties was observed instead. Poor layer to layer adhesion also contributed to the decrease in properties with a transverse force [13]. The research showed that adding the carbon fiber did improve the overall strength of the prints in the direction of the force load.

2.1.1. Fibers Types

Fibers can be classified into two different types, long and short: the difference between them is the aspect ratio. An aspect ratio is the difference between the diameter to overall length of the fiber. Typical aspect ratios for short fibers are between 20 and 50 and to be considered a long fiber the aspect ratio is between 200 and 500 [14]. Although long fibers in composites have higher mechanical properties, short fibers have a wide range of applications in engineering and are easier to process.

2.1.2. Long Fibers

Long fibers offer higher mechanical properties (e.g. tensile strength and Young's modulus) when combined into a composite. Long fibers can be found in a wide range of applications, from airplanes to ocean ships [15]. Long fibers add strength to composites. Because the fibers have a high aspect ratio, they give the matrix more area to attach onto, this allows for the transfer of force from the matrix to the fiber [16]. If the fibers are also aligned in the direction of the applied load, the fibers will absorb more of the force. Therefore, less force will be felt by the matrix material. Compared to metals, long fiber composites will be lighter, but still be able to perform the same objective. If a composite is made of long fibers instead of short fibers the effect of creep will also be lowered [17]. Creep is the sliding of polymer chains, which can break a composite. Creep occurs when a composite is under a load for an extended length of time. Long fibers help eliminate creep by stopping the propagation of cracks inside the composite.

When long fibers are added to a polymer matrix higher mechanical properties such as Young's modulus and tensile strength will increase [18]. Figure 6 below shows a qualitative description of how stiffness, strength, and toughness all increase with the length of the fiber.

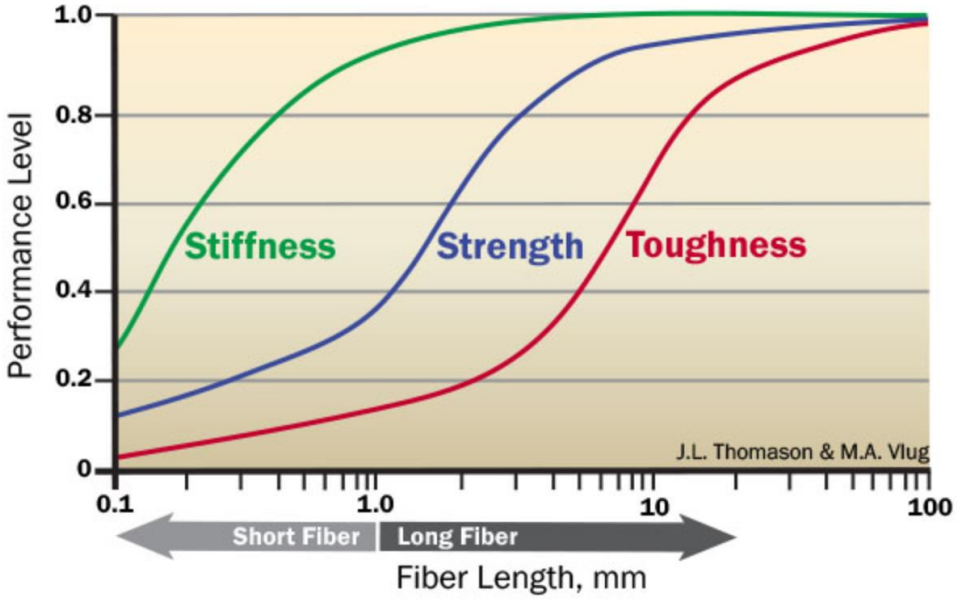

Figure 6: Qualitative view of fiber length and performance [19].

Long fibers may have an abundant amount of advantages, but they still present draw backs. Working with long fibers can be cumbersome and do not always align in the direction that is desired. When this happens, the mechanical properties that are expected fall short. Long fibers also can entangle with each other, which will make them extremely hard to pull apart or use in any real application. Fiber wet-out can also become a problem when using long fibers in a resin manufacturing process [20]. When the long fibers are not fully wetted out, the expected mechanical properties will not be optimal.

2.1.3. Short Fibers

Short fibers have better potential to be used in AM applications. Short fibers can be added to most applications that involve thermosets resins [21]. Unlike in long fiber composites, it is difficult to get the short fibers to align in a uniform direction. In the FDM printing type the

short fibers will align in random directions with no apparent order but will be distributed evenly through the composite. An example of this can be seen in Figure 7 below.

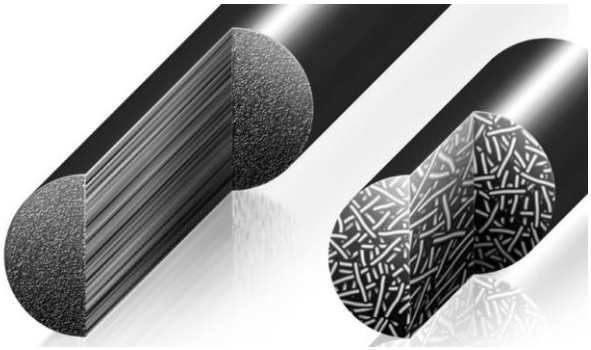

Figure 7: Difference in fiber direction of long and short fibers [22].

The versatility of short fiber is what makes them a great reinforcement to any matrix. It is easy to add them to most plastics, adding only 5% by weight can increase the mechanical properties of the original matrix by up to 25% [23]. There is a large range of different short fibers that can be used. The fibers with the highest tensile strength and Young's modulus are synthetic fibers, but natural fibers can be an inexpensive and effective alternative way to cut cost down and still improve the overall composite mechanical properties. As the cost of manufacturing increases, scientists and engineers are finding new materials to add to existing applications.

Short fibers can be used in many applications, but they still come with drawbacks. Adding short fibers to a matrix does improve the mechanical properties, but the improvement falls short in contrast to what long fibers can achieve. As the fiber length approaches the nano scale the fibers can agglomerate and act as a particle and not as a fiber. It is possible to keep these fibers apart, but special manufacturing process must be followed such as sonication. Not all properties are improved when using short fibers. If a large percent of the fibers are aligned in the transverse direction of the applied force the overall tensile strength can be decreased. The reason for this decrease in tensile strength is due to the force being applied in the transverse direction,

the effective cross-section area of the matrix is reduced from fiber voids. The matrix material has a lower tensile strength than the fibers and will now absorb the majority of the force [24].

Short fibers are a great reinforcement that can help improve the overall strength of a composite. Different fibers come with different properties. Understanding what fiber should be used will make the composite more efficient. When adding these fibers, it is important to know what mechanical properties the user is trying to improve such as: strength, stiffness, conductivity, etc. Combining two different fibers in a matrix can also make for unique properties that might not be achieved with a single fiber choice. Short fiber composite may not exhibit as high of properties as long fiber composites but, will still always have a place in engineering.

2.2. Combining Research

The Army Research Lab (ARL) first started this project in hopes that someday a 3D printer would accompany a platoon of soldiers in the battlefield. The 3D printers would then be used to manufacture unmanned aerial intelligence surveillance reconnaissance (ISR). These robots could then be used to fix broken vehicles [25]. If this was possible, it could limit the number of soldiers in any battlefield and lower the chances of causalities. Originally the project was to design a tougher resin, but as the research progressed a different avenue was taken, because of this combining UV resin and short fibers was created.

2.2.1. Previous SLA Reinforcement Studies

As stated earlier, Simpson [6] was able to combine 5% by volume of carbon fiber with a UV resin. Two major problems came from this. First, the carbon fiber was opaque to UV light and second, the thermal initiator that was added created void bubbles that lead to stress concentration points. It is also worth noting that Simpson [6] was unable to successfully print with a volume fraction higher than 5%. One of the advantages found was that the carbon fiber

would suspend itself in the resin because both the resin and the carbon fiber had similar densities. This allowed for a uniform dispersion of fiber throughout the printed part. To optimize his prints Simpson [6] made three different print orientations. This can be seen in Figure 8 below.

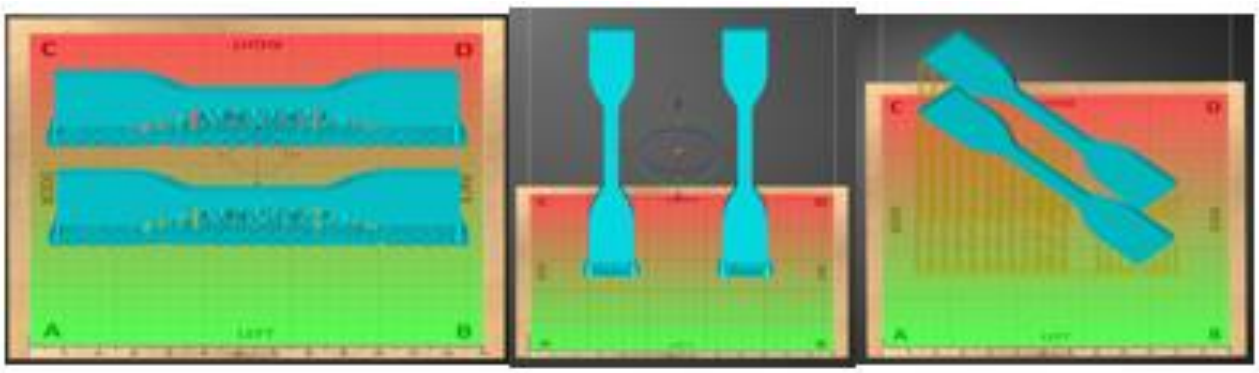

Figure 8: Print orientation at angle 0°, 90°, and 45° respectively [6].

All three print orientations had similar Young's modulus and tensile strength. Printing at 45°, there had to be a large number of stilts printed with the tensile samples, this led to unneeded stress formed during the peel step.

2.2.2. Evolution of SLA Short Fiber Reinforcement

After examining the past research, the disadvantages that carbon fiber imposed was too large to overcome. The opaque characteristic of carbon fiber could not be changed and therefore not used to further the project. With the elimination of carbon fiber, a new reinforcement was needed to be selected, glass fiber was the next best choice. The research done by Simpson [6] was replicated only to the extent of using the same printer and dimensions of the printed samples. This was to potentially compare results of both studies.

2.2.3. Glass Fiber

2.2.3.1. Transparency

Glass fiber is more than 75% transparent to UV light. This characteristic led to elimination of post curing with a thermal initiator [26]. Without a post cure process the presents of voids would be eliminated.

2.2.3.2. Fiber Size

It is not possible to add long fibers to the UV resin mix and still be able to print easily. Because of this a short fiber had to be used. The fiber selected had to be able to flow through a 6.4 mm diameter tubing and not hinder the flow or cause blockage. The fiber size used came in a range with a maximum length of 0.8 mm and minimum length of being considered a particle. The average length was 230 μm and aspect ratio of 1:5. As the fiber flows through the hosing there is no settling of the fibers and does not hinder the flow. The increase in viscosity of the mixed resin also did not hinder the pump and could continuously pump for over 4 hr without difficulties.

2.2.3.3. Strength

Glass fiber has been used in varying engineering applications. Its mechanical properties are lower than carbon fiber, but still produce high mechanical strengths. Glass fibers are commonly manufactured in three different types: A glass, S glass, and E glass [27]. A glass is short for alkali glass and is commonly used to make jars, containers, and bottles for liquid beverages. A glass is not commonly used in fiber reinforcement; therefore, it was not considered for this research. S glass, or structural glass, has the highest mechanical properties among the different types of glass fibers. Being the strongest, it can be hard to come by because it is used in such a large variety of applications. Because of this, it too was not considered for this research as

well. E glass, or electrical glass, is a unique balance between cost and performance. This type of glass is commonly used in aerospace composites and marine applications. It is very easy to buy E glass in most lengths and in large qualities. E glass' moderate to high mechanical properties and availability made it the best choice for this research. In future research S glass should be considered because S glass does exhibit highest mechanical properties.

2.3. Flow Fields

2.3.1. Glass Fiber Sinking Rate

The glass fibers used in this research had a density of $2.57\ g/cm^3$, more than twice the density of the resin at $1.084\ g/cm^3$. Simpson [6] found that carbon fibers could be suspended in the resin long enough for the print a uniform distribution throughout the prints. In contrast, glass fibers were so dense that the fibers would begin to sink immediately. Figure 9 shows a gradient of fibers over the print.

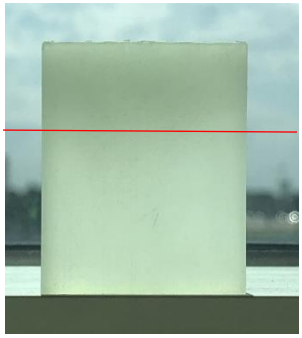

Figure 9: Fiber dispersion gradient of non-pumped sample.

The section above the red line show what was printed first. Above the red line the specimen is darker in color indicating that more glass fiber is present, as the print continued the fibers began to sink. As the fibers began to sink a gradient could be seen. The results and conclusions regarding the rate of fiber sinking will be discussed later in this thesis. A small pool of only resin forms as printing continues. Once the fibers have completely sunk to the bottom of resin tank the remaining section can be considered neat. This can be seen in the Figure 10 below.

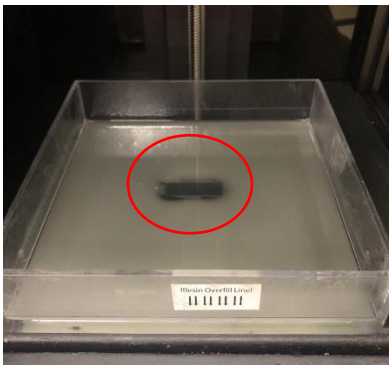

Figure 10: Pooling of resin where sample was printed showing no fiber being present.

This small pool would form during printing because the fibers would congeal at the bottom of the tank and not be able to flow under the print. Tensile dog bones shaped samples were printed first and tested. There was a small increase in Young's modulus and small decrease in tensile strength. It was easy to conclude that the fiber was not fully present in the gauge section of the print. A density check was also completed from different parts of the dog bone sample. Density testing results will be discussed later in the thesis.

3. OBJECTIVE

The low mechanical properties of acrylate based curable UV resins makes the application of 3D printing only useful in prototyping and small industry applications. Increasing the mechanical properties could potentially expand these possibilities. Adding glass fiber as a reinforcement to the UV curable resin could increase properties such as: Young's modulus and fracture toughness. Adding a flow field in the resin tank could create a more isotropic material and better fiber dispersion.

The objective of this research was to determine if the addition of glass fibers increased the overall mechanical properties of the composite. To accomplish this objective, three goals were set: 1) Determine if adding a flow field in the resin tank increased the overall dispersion of the fibers in the composite, 2) Examine the fiber dispersion and gradient inside the prints, and 3) Evaluate the mechanical properties of the prints using various tensile and flexural tests.

4. PROCESSING

The glass fibers are nearly twice as dense as compared to the UV resin matrix. Because of this large density difference the glass fiber begins to sink immediately and within a couple of minutes, all the glass fibers will be on the bottom of resin tank. A way to suspend the fibers in the UV resin had to be found if they were to be added to the resin. To accomplish this a flow field was created throughout the resin tank. As the fibers stayed suspended, the prints would exhibit no gradient of fiber. The preparation of the fiber, resin, resin tank, final cure, and printer all had to be customized.

4.1. Mixing

The glass fibers are difficult to evenly spread into the resin medium. As the fibers are poured into a beaker they agglomerate and become difficult to break apart. These agglomerations will then float near the top of the resin surface, to fix this problem, a twostep process was developed to ensure an even spread of glass fibers.

4.1.1. Step Process

If only a planetary mixing apparatus was placed in the glass fiber and UV resin mixture the twisting head would not move. First, the large agglomerations of glass fiber had to be diminished. Second, the large agglomerations had to be broken apart with a plastic stirring rod for 2 min. Once all the large particles were broken up, the beaker would be place under a TALBOYS Laboratory Stirrer model number 103 with a three blade spinning head. The stirrer can be seen in the Figure 11 below.

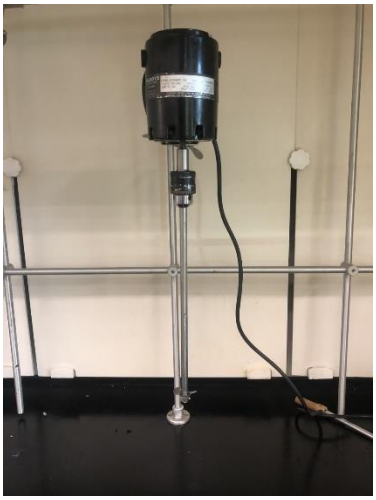

Figure 11: TALBOY Laboratory Stirrer.

The combination of the UV resin and glass fibers increased viscosity and the beaker had to be secured to the table. The combination of UV resin and glass fibers would then be placed in the stirrer for 15 min at 2000 rpm. As the agglomerations of glass fibers dissipated, the color of the liquid would change from a clear resin with white dots to a consistent light gray color.

4.2. Degassing

The UV resin and glass fiber were mixed so aggressively that air bubbles would get entrapped in the mixture. If the bubbles were not removed, either the samples would be unsuccessful and fail to print, or samples would under preform during testing. Previous research concluded that these small voids would hinder the overall mechanical properties of the prints [8].

4.2.1. Vacuum Chamber

The vacuum chamber used in this process was a two-part system that had an external pump attached to a vacuum oven chamber. The pump and vacuum oven chamber can be seen below in Figure 12.

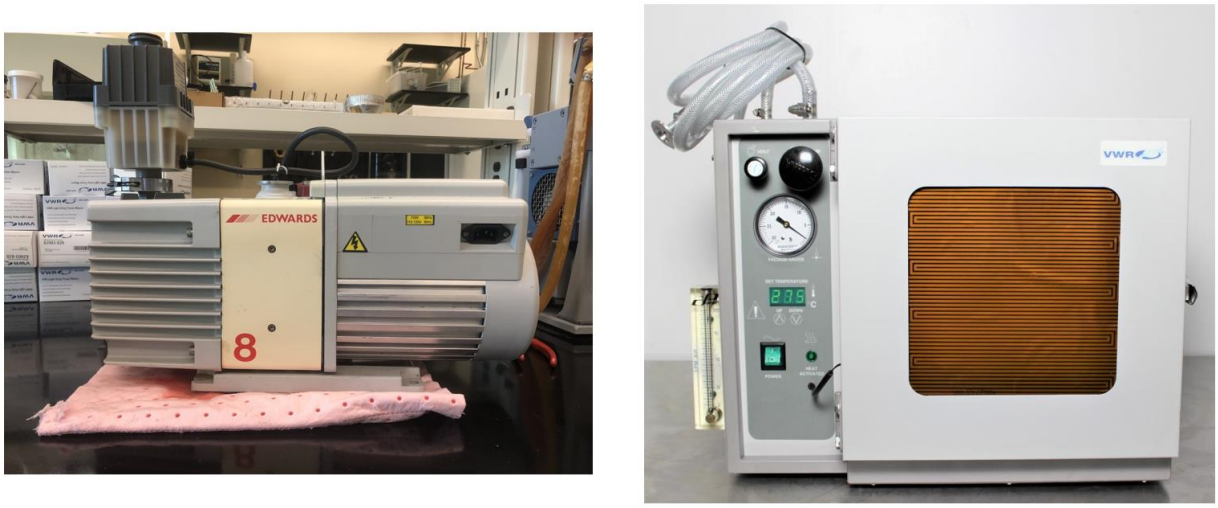

Figure 12: Pump and vacuum oven chamber [28].

The pump used was an Edwards model number RV8 and the vacuum oven chamber and a VWR Industries Vacuum Oven Chamber model 1415M. The glass fiber resin mixture was prone to foaming at high vacuum pressure. If the vacuum pressure was too low the majority of the bubbles would not retreat from the mixture. To make sure all the air bubbles left the mixture, a vacuum pressure of 15 mmHg was kept for 20 min. At this pressure and time interval, it was clear to see the bubbles evaporated from the mixture. Once all the air was out of the mixture the UV resin and glass fiber mixture would change colors again from a light gray to a darker gray. It is important to note that the mixture would change this color 15 min in the vacuum cycle but to ensure the elimination of all air the mixture was kept in the vacuum chamber for an additional 5 min.

4.3. Printer and Process

The printer used in this research was a Moai 130 inverted SLA printer. This type of printer was chosen because of the ability to customize the printer settings. Brands such as FormLabs are not open source and because of this, the printer settings cannot be changed by the user. It was very important to be able to change different settings of the print because the resin

was not the only medium being printed. The Moai 130 inverted SLA printer can be seen below in Figure 13.

Figure 13: Moai 130 inverted SLA printer [29].

The most important setting that had to be changed was the speed of permanent magnet (PM) motor which controlled the speed at which the resin tank would tilt during the peel step on the x-axis. The PM motor speed was slowed to ensure that the maximum amount of UV resin and glass fiber mixture could travel under the build plate.

4.3.1. Pump Selection

The mixture of UV resin and glass fiber had to be continually flowing. If not, the glass fiber would sink to the bottom of the resin tank. A DC 12 V Vacuum Pump Strong Suction Self-Priming Peristaltic Pump was used to achieve the flow needed. This pump can be seen in Figure 14 below.

Figure 14: Peristaltic pump used to create flow [30].

Using a peristaltic pump has many advantages in this application. First, the assembly of this type of pump is very simple which allowed for the pumping system to be cleaned easily. After each print, the head of the pump had to be detached and the hosing had to be cleaned or thrown away. Second, the motor never came in contact with the working fluid. The UV resin and glass fiber would have been corrosive on the motor and scratched or broken the moving parts. The pump was connected to a 12 V 55 A hr. battery. At max output the motor could achieve 400 ml/min with a hose inner diameter (ID) of 6.4 mm.

4.3.2. Printer and Pump Setup

The resin tank in the Moai 130 SLA printer had to be modified to allow for a flow field. To do this, four holes were drilled, two in the front and two in the back, the holes were 5 cm from the edge of the resin tank. Inlet and outlet ports were then glued to the holes and hosing then connected to the inlets, outlets and the pump. A diagram and picture setup can be seen in Figure 15 below.

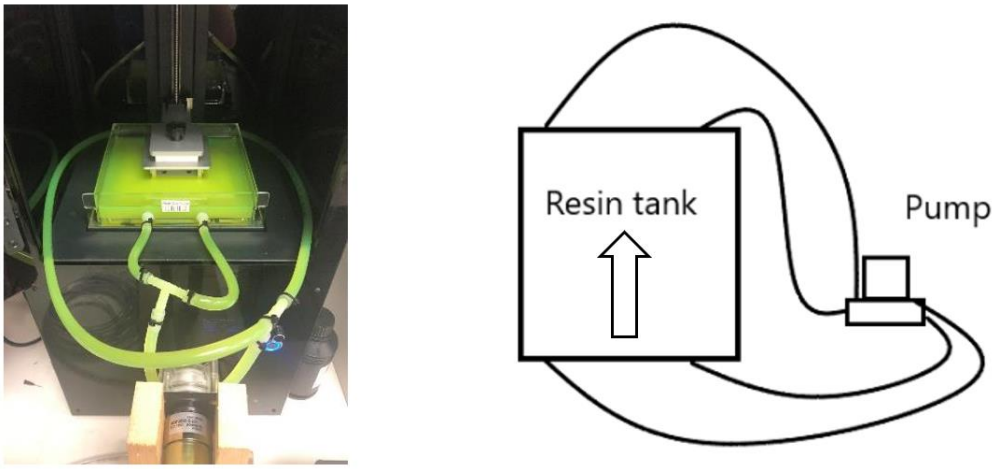

Figure 15: Diagrams of pumping setup.

The UV resin and glass fiber mixture were pumped from the front of the resin tank to the back, all samples had the same flow direction. Green resin was not used in any tests but was used to show the setup. All connections were secured with zip ties so there would be no leakage or disconnections.

4.4. Materials

Two materials were utilized in this study. The first was Peopoly UV resin and second was 1/32 inch (0.8 mm) milled E glass fiber. Both can be seen below in Figure 16.

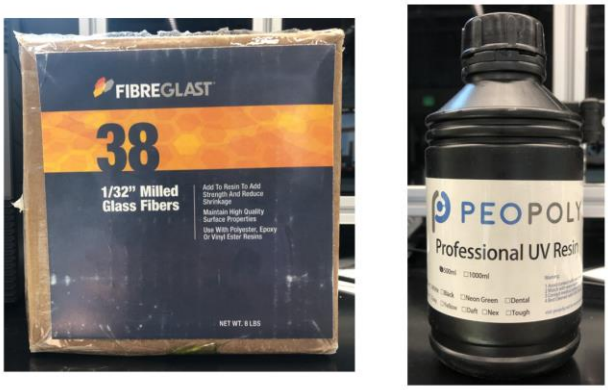

Figure 16: 1/32 inch Milled Glass fibers and Peopoly UV Resin.

The glass fiber was purchased from Fibre Glast Development Corporation. The resin was purchased from Peopoly. The data sheet for the glass fiber indicated the fiber had a mean length

on 1/32 inch (0.8 mm), aspect ratio of 1:16, and a cationic sizing agent [31]. The exact sizing agent used on these glass fibers was not able to be found, the manufacture only stated the sizing as cationic and designed from epoxy based resins. One of the most used sizing agents used on glass fiber is aminopropyl triethoxy silane, which can be easily turned cationic [32]. This compound is also used regularly on E-glass fibers. After observing the glass fibers under a microscope it was determined that the true mean length was closer to 230 μm and an aspect ratio of 1:5. Upon further investigation and communication with the manufacturer, the mean length and aspect ratio are different because the manufacture used a 1/32 inch (0.8 mm sieve), meaning that all particles that size or smaller fall through the holes. The UV resin used was standard Peopoly's acrylic based UV SLA resin.

4.4.1. Material Choice Reasoning

The 1/32 inch (0.8 mm) milled E glass was chosen for two reasons. The first, E glass is a strong milled glass, easiest to purchase, and retains high mechanical properties. Second, fiber longer than 1/32 inch (0.8 mm) had the potential to build up and clog the 6.4 mm diameter hosing used.

The Moai printer used was manufactured by Peopoly. This company also produces their own resin and recommended that resin be used with their printers. For this reason, the standard Clear Peopoly UV resin was used in these experiments.

4.5. Post Cure

Immediately after the printing process was complete, the prints where washed with 95% ethanol to remove and any UV resin build up. The supports of the prints were also kept in place until after being heated in the UV oven.

To ensure a full cure, all prints were placed in a UV oven for 60 min. The oven consisted of three 25 W LED UV lights, a heating element, and a rotating base. The rotation of the bed allowed for all side of the prints to be illuminated by the UV Lights. A picture of this can be seen in Figure 17 below.

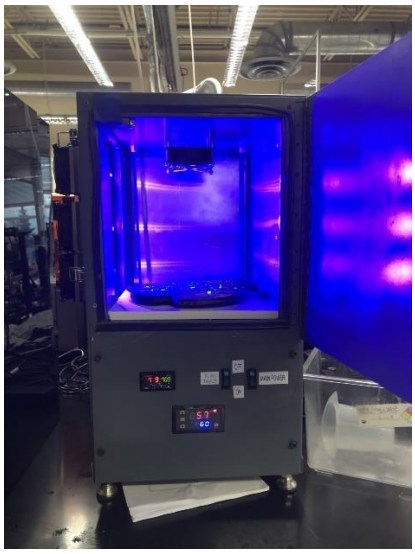

Figure 17: Post curing UV oven.

4.6. Surface Roughness

The surface finish of the print will impact the mechanical properties of each specimen. Three concerns become apparent when examining the final printed parts. First, the overall surface has a very rough and sandpaper-like feeling; glass fibers are inherently rough. When printing a number of the glass fiber are not entirely in the diameter of the laser and protrude slightly out of the shape of the original print. This can be seen below in Figure 18.

Figure 18: Surface roughness of tensile sample.

In Figure 18, the white parts that can be seen are the fibers protruding out from the original print. Overall, this has not been a large problem. In the future, it may be hard to refine prints that are required to exhibit a high-quality surface finish.

Curved edges can be difficult for SLA printers. As each layer is printed a small edge can be formed. These edges can become a major problem with testing. In Figure 19, there is a curved portion of a dog bone tensile sample, the small white lines are layers of the print. Each one of these lines can create a stress concentration point. While testing, it was also observed that some of the samples would break close to the curved portion of the sample instead of flat gauge section. When this happens, the true tensile strength can be difficult to determine.

Figure 19: Noticeable layering of poor curve from printing of a tensile test sample.

Support structures must be made in order to hold the specimen as it is being printed and before testing can occur, these supports must be removed. The process of extracting the specimen from the supports can be harsh on the integrity of the specimen. The supports are cured

onto the specimen. To remove the supports, first they must be carefully broken off and then sanded to make them flat. It can be very difficult to make the specimen completely flat resulting in dimpling. This can be seen below in Figure 20.

Figure 20: Dimpling on gauge section of tensile sample.

The dimples can also create stress concentration points similar to the layer-to-layer curving. Sanding helped to remove the dimple, but only so much can be removed before other problems arise such as curving the gauge section or putting too much stress on the gauge section while sanding. The prints were first sanded with a 60-grit piece of sandpaper to remove the larder dimples, followed by a 150-grit to smooth the surface.

5. TESTING

Computational Fluid Dynamics (CFD) simulations and a series of five different testing procedures were conducted on the printed samples. The five were: gradient and density testing, Dynamic Mechanical Analysis (DMA), tensile testing, flexure testing and notched fracture testing. These tests were performed to find unity in printed parts and to determine which mechanical properties changed with the added glass fiber.

5.1. CFD

Computation Fluid Dynamics is a powerful tool that allows the user to see different flow lines and the velocity in a working fluid. Using CFD, 14 different cases were examined to determine if flow acted in aligning the fiber. All simulations were conducted using a flow rate of 3.52 g/s, based off the flow rate of the pump and density of UV resin and glass fiber mixer. All the simulations had the same boundaries conditions of a five-sided box with the top open. A tetrahedral element type was used to ensure a high-quality simulation. Each simulation varied on the total number of elements, the simulations that involved samples printing at 0 μm and 100 μm from the bottom of the resin tank had a total element count around 705,000. The simulations where the samples are angled had an element count around 2,330,000.

Figure 21 below shows the exact dimensions 166 x 166 x 20 mm which matched the resin tank of the Moai printer. In the Figure, eight different ports can be seen. Transverse and parallel prints to the flow were examined, to do this opposite inlets and outlets were turned on or off.

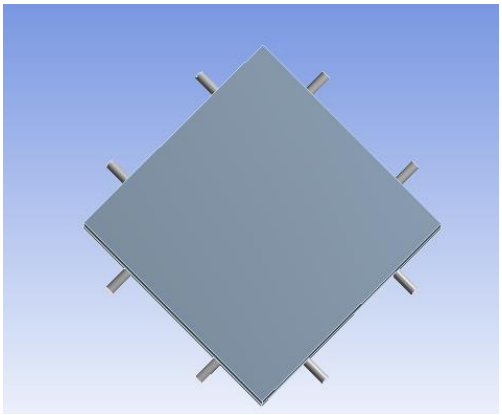

Figure 21: Constrained volume with inlets and outlets of UV resin tank.

5.2. Density and Gradient

Without a flow field present in the resin tank the glass fiber began to sink within minutes. Visual tests and density calculations were performed to ensure the fibers were an evenly spread. An Ohaus Adventurer scale was used to weigh four pieces from four different sample pieces. Using a Mettler Toledo density determination kit, the densities of all the samples were recorded. A picture of this setup can be seen below in Figure 22.

Figure 22: Ohaus Adventurer scale and a Mettler Toledo density determination kit combined to find sample density.

5.3. Viscosity Testing

A viscosity test was performed using a Brookfield DV-II+ Pro Viscometer. This test was needed to determine if the fluid would be too viscous for the pump to handle, Figure 23 below is a picture of the machine used.

Figure 23: Brookfield DV-II+ Pro Viscometer.

5.4. Dynamic Mechanical Analysis (DMA)

DMA was performed to evaluate whether a similar degree of cure was achieved between the neat resin samples and the glass fiber reinforced composites. To perform this, ASTM D5418-15 [33] was followed. Three samples of both neat and glass fiber reinforced were needed for this test, using the dual cantilever mode DMA. Each sample was printed at 60 x 13 x 4 mm to fix in the dual cantilever grips. The test parameters went as follows: temperature range of 30 °C to 150 °C, with a frequency of 1 Hz, amplitude of 15 µm, and a heating rate of 1 °C/min. A TA Instruments DISCOVERY DMA850 was used and can be seen in Figure 24 below.

Figure 24: TA Instrument DISCOVERY DMA850.

5.5. Tensile Testing

Three print orientations were manufactured and tested. This was done to determine if different orientations could induce alignment of the glass fibers. There is no direct ASTM standard for 3D printed parts. A combination of both ASTM D638 [34] and ASTM 3039 [35] were considered. Five samples in each orientation, five neat samples, and five samples without a pump system were tested. The dimensions and print orientation can be seen in Figure 25.

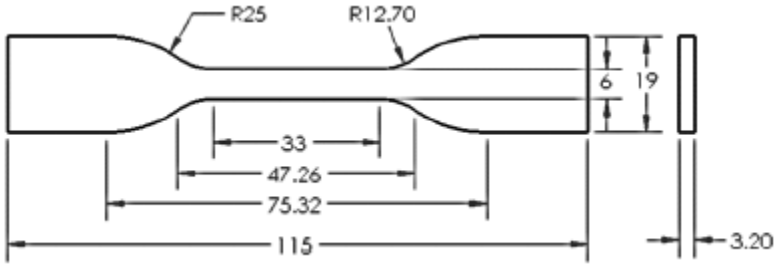

Figure 25: Print dimensions for tensile testing in mm [6].

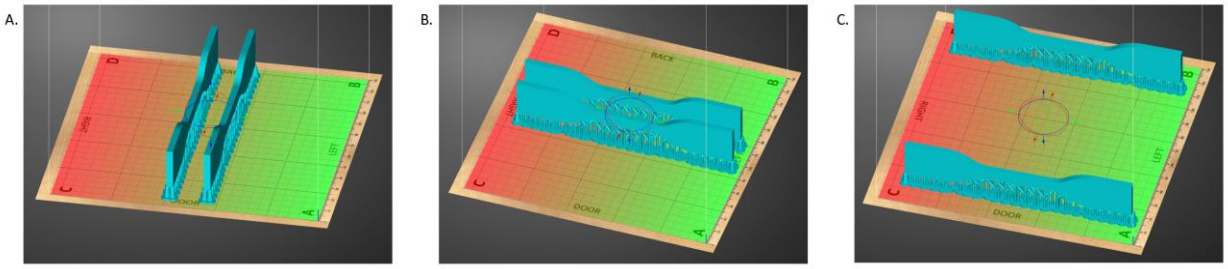

Figure 26: Different print orientations used for tensile testing.

Figure 26 shows the print orientation, picture A has the tensile samples parallel with the flow and 1 cm apart, this printing orientations will be denoted as Para-flow (PF). Picture B has the samples in the transverse direction of the flow and 1cm apart, this printing orientations will be denoted as Trans-flow (TF). Picture C has the prints in the transverse direction of the flow and 4 cm apart, this printing orientations will be denoted as Trans-flow-wide (TFW). Bluehill Software was used to control the load frame. Figure 27 below shows the Instron 5567 load frame used in the tensile test with a sample in the grips.

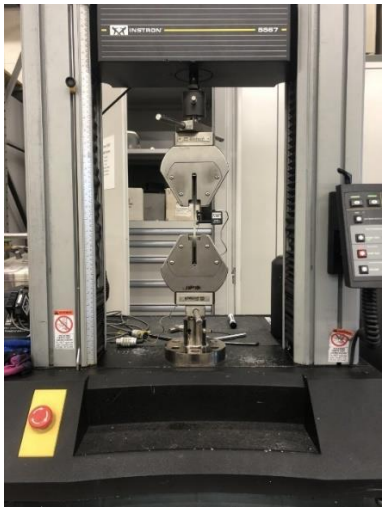

Figure 27: Instron 5567 Load Frame setup for tensile testing.

5.6. Flexure Testing

Similar to tensile testing there is no direct ASTM standard for 3D printed parts, therefore ASTM D790 [36] was used. The dimensions of the samples can be seen in Figure 28.

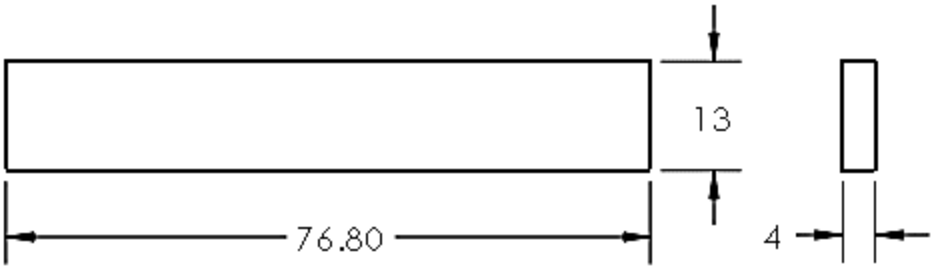

Figure 28: Dimensions of flexure samples in mm [6].

Flexural testing was also performed on the Instron 5567 and controlled by Bluehill software. The print orientation used was in parallel with the flow, five neat samples and five glass fiber reinforced samples were tested. This can be seen in Figure 29 below.

Figure 29: Instron load frame setup for flexural testing.

5.7. Notch Fracture Toughness

The last mechanical testing conducted on the samples was a notch fracture test to find the fracture toughness. This test was carried out using the ASTM D5045 standard [37], Instron 5567, and controlled by Bluehill software. Two possible ways to make these samples where considered. First, print the notch in the sample, and second, use an end mill to remove material to

notch the sample. The latter of the two was eventually selected. This was decided because when the parts cure in the oven they shrink. As this happens there is a chance for residual stress to act on the samples. This reason made milling was the better option. Three neat and three reinforced samples were tested. The testing setup was similar to flexure testing. In this fracture toughness testing the notch was faced down.

5.8. Scanning Electron Microscope Images (SEM)

A scanning electron microscope was used to find quality of the prints and fiber pull out. Multiple samples from print orientations PF, TF, and TFW were examined. The surfaces examine included, down the longitudinal edge of the glass fiber reinforced tensile samples, on the fracture surface of the glass fiber tensile samples of glass reinforced, and on the fracture surface of the neat flexure sample. To prepare for SEM images, first the samples where coated in a conductive layer of gold using a Cressington 108 auto sputter coater. From here, the coated samples where attached to a cylindrical aluminum mount with a colloidal-silver paste. To obtained images a JEOL JSM-6490LV scanning electron microscope operating at an accelerating voltage of 15kV was used. A view of the tensile samples can be seen below in Figure 30 and Figure 31.

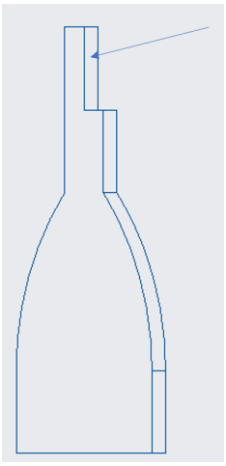

Figure 30: Diagram of longitudinal axis of tensile sample showing were SEM images were taken.

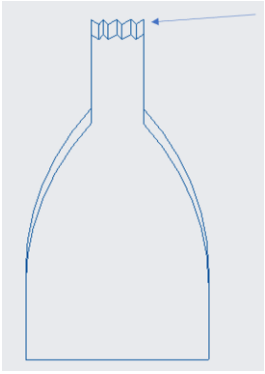

Figure 31: Fracture surface of tensile sample scanned for SEM images.

6. RESULTS

6.1. CFD

The results of the following simulations helped to show where the streamlines appeared. It was important show whether the streamlines travelled underneath the specimens being printed or whether the streamlines travelled around the specimens.

A baseline was needed in order to show the flow field when only the UV resin was present in the resin tank. This was important because being able to see if there was a flow to begin with would determine if more simulations where needed. Figure 33 below shows the flow when only the UV resin and glass fibers are present in the tank without an object being printed.

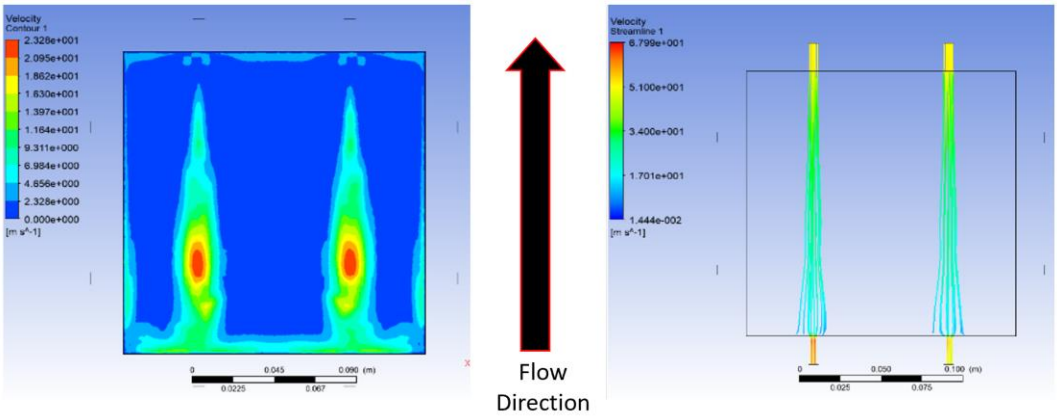

Figure 32: Baseline of resin tank filled only with UV resin and glass fibers.

From this simulation, the highest flow velocity was observed in the front quarter of the resin tank. As the velocity decreased the streamlines stayed constant until the latter quarter of the resin tank. To try to improve the back quarter of the resin flow the simulation was changed to have the outlet double its flow rate to try and have a more constant streamline velocity. Figure 33 below shows this simulation.

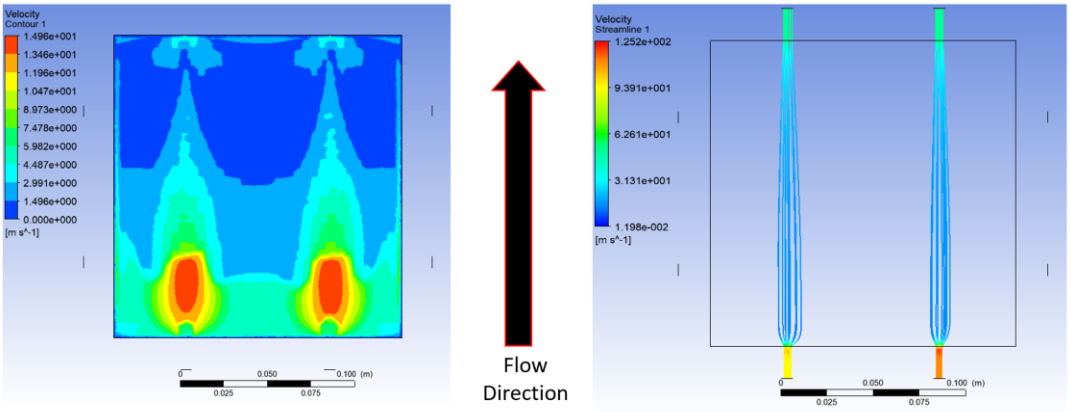

Figure 33: Doubled outlet flow rate of baseline with only UV resin and glass fibers.

The streamlines in this simulation have a constant velocity but achieving this would be difficult and ultimately not work as the inlet would not be able to keep the resin tank full. This idea was abandoned, and the original simulation was used.

6.1.1. Printed Parts and Flow Field

Three different simulations were conducted for each print orientation. Tensile samples were printed in two different orientations with flexural in one thus producing another 12 simulations. All simulations were designed so that the printed part is halfway through its printing process. The reason for three different simulations for each orientation was to show the flow field at the three most important positions of the print. The first position simulated had samples 100 μm from the bottom of the resin tank, the second position had samples in contact with the resin tank bed simulating a complete layer and the last position is at the maximum angle during the peel step.

6.1.2. Results from CFD

The results from the CFD testing showed that the flow went around the printed samples. There were a low number of streamlines that penetrated through the supports, but over-all the flow travelled around the samples. Even with the difference in length and size both the tensile

and flexural samples' streamline showed the same trend. When the samples were at 100 μm off the bottom of the bed, there was not enough room for the flow to travel underneath. This was also observed when the samples were in contact with the bottom of the resin tank, again the same streamlines were observed. At the largest angle of the peel step, the flow still travelled around the samples instead of under. These results are the same for parts printed both transverse to and parallel to the flow. Theses simulations can be seen in the Appendix under A.1 through A.12.

6.2. Viscosity

It was found that the viscosity of the neat resin was 517 cP and, the combination of glass fiber and resin mixture had viscosity was 950 cP. When adding 15% by volume of glass fiber, the viscosity of the mixture increased by 45%. No other fiber amounts were tested because only 15% by volume of glass fiber was used. The pump motor used was able to work without any problems if the total working time was less than 4 hr. If the print time lasted long that 4 hr the pump motor would begin to heat up. The print time for the longest print was only 2.5 hr. Therefore, the mixture having a viscosity of 950 cP was not deemed a problem.

6.3. Density Testing and Fiber Percent

Three different fiber by volume percentages were examined. A MatLab code was designed to be able to convert from fiber volume to fiber mass. The reason for this was to be able to weight the fibers and UV resin allowing for a more accurate measurement, this MatLab code can be seen in Appendix A.29. The first fiber percent examined was 5%. The initial prints were successful but after tensile testing only a small increase in Young's modulus was observed. The variability in the neat samples made it difficult to find an exact percent increase because of the large standard deviation. The next fiber volume percent trialed was 15%. At this percent it was easier to find the trend of increase Young's modulus. The last percent by volume used was 25%.

The prints were successful at this percent as well, but a large amount of glass fiber was needed for every print. Because of this, the percent used in this research ultimately was 15%.

The density of the composite changed from the top of the print to the bottom of the sample when no pump system was present. When examining the samples, a gradient of fibers/density could easily be seen without a microscope. Table 1 shows the densities averages and whether a gradient was observed.

Table 1: Densities of specimens examined.

Process	Density g/cm^3	Gradient
No pumping	1.26	Yes
Pumped Sample 1 Edge	1.39	No
Pumped Sample 2 Middle	1.40	No
Pumped Sample 3 far Edge	1.39	No

The theoretical density of the composite based on the rule-of-mixtures, assuming no voids, was 1.42 g/cm^3. The three samples that used the pumping system only had a 1.4% deviation. Since this deviation is so small, it can be assumed the samples that printed with the pumping system are evenly distributed. Below in Figure 34 are two pictures that help show this gradient.

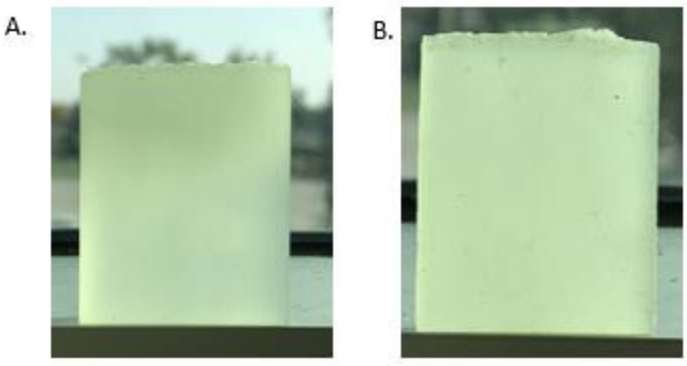

Figure 34: Sample printed without a flow field (A) and a sample printed with a flow field (B).

Picture A shows a rectangle sample that was printed without the pumping system. The section at the top of the rectangle was printed first and shows that there is glass fiber present, but around the middle of the print all the glass fibers have sunk to the bottom of the bath. Because of this, the glass fibers where no longer being incorporated into the print. Picture B was printed using the pumping system and shows no gradient of the print and has consistent fiber dispersion throughout.

6.4. DMA

To assess potential differences in the amount of cure in the samples, DMA was performed. The glass transition temperature (T_g) was found using the tan δ curve. This was then used to determine if the glass reinforced samples had been optimally cured to the same degree as that of the neat sample. The neat resin was considered to be optimally cured to be compared to the reinforced resin glass fiber composite. When examining the curves of the neat samples the average T_g was found to 107.59 °C. Sample 3 had close to the actual T_g and can be seen below in Figure 35.

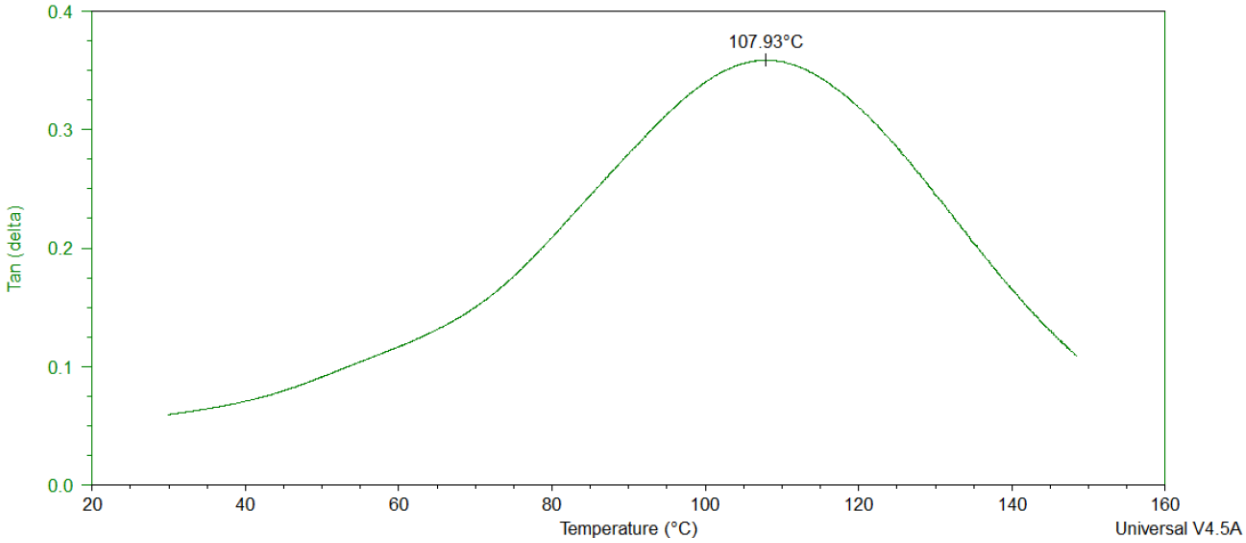

Figure 35: Neat sample 3 of DMA testing.

When the T_g of the neat samples was found the next step was to print and find the T_g of the glass reinforced samples. Three more samples where tested having an average T_g of 109.19 °C. Glass sample 1 had the closest T_g to this value and the graph can be seen below in Figure 36.

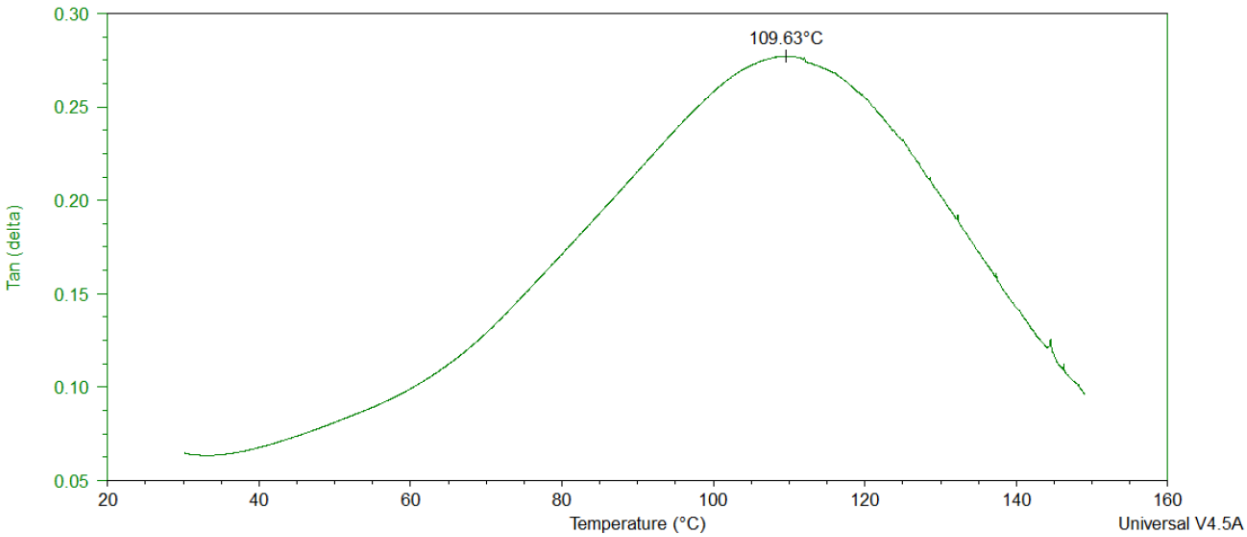

Figure 36: Glass sample 1 of DMA Testing.

When adding a reinforcement such as glass to a polymer matrix it is expected to see an increase in the T_g. It was found that by adding the glass fiber to the resin matrix the T_g increased by 1.6 °C. This increase in T_g illustrates that both the neat and glass reinforced samples have a similar cure.

6.5. Tensile Testing

A baseline had to be established in order to compare results of neat, glass fiber reinforced without a pumping system and glass fiber reinforced with a pumping system. Three main mechanical properties were examined, Young's modulus, tensile strength, and strain-to-failure. A graph of the neat tensile strength, Young's modulus, and strain-to-failure samples can be seen in the Appendix A.13, graph of the Young modulus samples can be seen in A.14 and the graph of strain-to-failure can be seen in A.25. The stress vs. strain curves of these samples can be found in the appendix as A.33.

The first was a baseline of the neat resin samples. The second baseline was to show results of the resin and glass fiber mixed but without a pumping system (NP). This was performed to determine if the addition of glass fibers increased or decreased tensile properties. Again, tensile strength, Young's modulus, and strain-to-failure were examined. The stress vs. strain curve can be seen in appendix A.32. The neat and no pump samples were printed in the PF orientation. The graphs for these test samples can be seen in the Appendix under A.15, A.16 and A.26. The stress vs. strain curves of the samples can also be found in the Appendix A.34.

The first printed samples were also printed in the PF orientation. When doing this, 15 % glass fiber by volume was added to the neat resin and resulted in a 20.9 % decrease in tensile strength, a 57.3% increase in Young's modulus and a 23% decrease in strain-to-failure. The decrease in strain-to-failure was expected as the Young's modulus increased. The decrease in tensile strength can be explained by fibers aligning in the transverse direction of the force or a agglomeration of fibers in a small area. When this happens the fiber acts as a void and does not help distribute the force. The theoretical Young's modulus can be determined by the Halpin-Tsai micromechanical models. To determining longitudinal modulus equation 6.1 was used below,

$$E_L = \left[\frac{1+\left(\frac{2l}{d}\right)\eta_L V_f}{1-\eta_L V_f}\right] E_m \tag{6.1}$$

To determining the transverse modulus Equation 6.2 below was used,

$$E_T = \left[\frac{1+2\eta_T V_f}{1-\eta_L V_f}\right] E_m \tag{6.2}$$

from here both equations 6.3 and 6.4 will be needed to find the theoretical Young's modulus.

$$\eta_L = \frac{\left(\frac{E_f}{E_m}\right)-1}{\left(\frac{E_f}{E_m}\right)+2\left(\frac{l}{d}\right)} \tag{6.3}$$

$$\eta_L = \frac{\left(\frac{E_f}{E_m}\right)-1}{\left(\frac{E_f}{E_m}\right)+2} \tag{6.4}$$

In the equations above, E_m represents the Young's modulus of the matrix, E_f represents the Young's modulus of the fiber, l is the fiber length, d is the diameter of the fiber, and V_f is the fiber volume constant. When using the above equations, the Young's modulus E_r of the composite can be determine using equation 6.5 below.

$$E_r = \frac{3}{8}E_L + \frac{5}{8}E_T \tag{6.5}$$

Using this formula, the theoretical randomly oriented fiber reinforced composites should have a Young's modulus of 3.98 GPa [38].

When looking at the CFD with no parts being printed, the flow was at its maximum closer to the middle of the print bed. From here, print orientation TF was developed in hopes to have more random fiber orientation. The graphs of the tensile strength, Young's modulus, and strain-to-failure samples can be seen in the appendix under A.17, A.18 and A.27. The stress vs. strain curves of these samples can be seen in the Appendix A.35.

Printing in TF orientation increased the Young's modulus but decreased the tensile strength. The Young's modulus was increased 77% on average from neat samples, the tensile strength decreased by 36%, and a decrease in strain-to-failure of 37%. Trying to print where flow is the maximum, print orientation TFW was developed and used. The results of each sample can be seen in the Appendix under A.19, A.20, and A.28. The stress vs. strain curves of these samples can be seen in the Appendix A.36.

In the TFW orientation, the Young's modulus was at its lowest with only a 44% increase, there was less of a decrease in tensile strength with only a decrease of 33%, a decrease of 30% was also observed for strain-to-failure.

Out of the three different print orientation, TF orientation had the highest Young's modulus, the lowest tensile strength, and lowest strain-to-failure. Where print orientation PF had the highest tensile strength. These results can be seen next to the neat samples and no pump samples in Figure 37, Figure 38, and Figure 39 below. The average stress vs. strain curve of each print orientation as well as neat and no pumping system can be seen Figure 40.

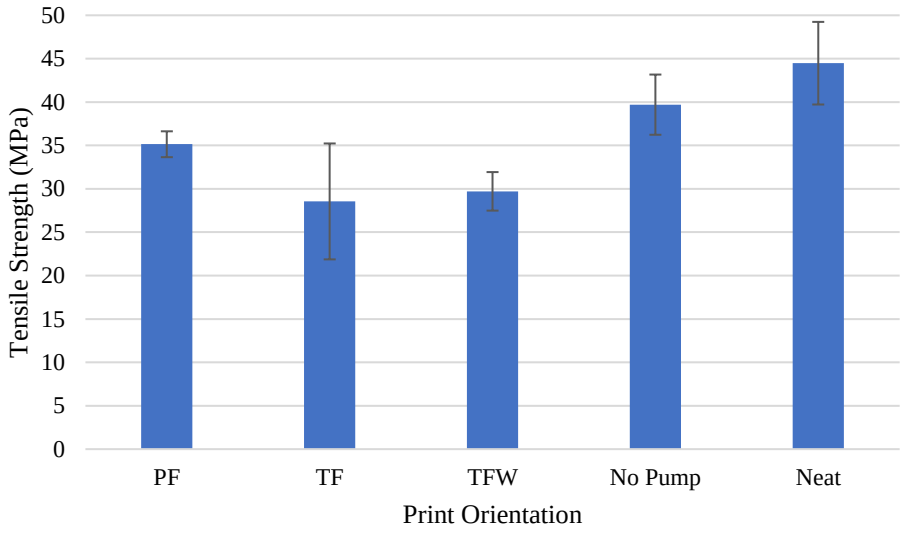

Figure 37: Average tensile strength of samples.

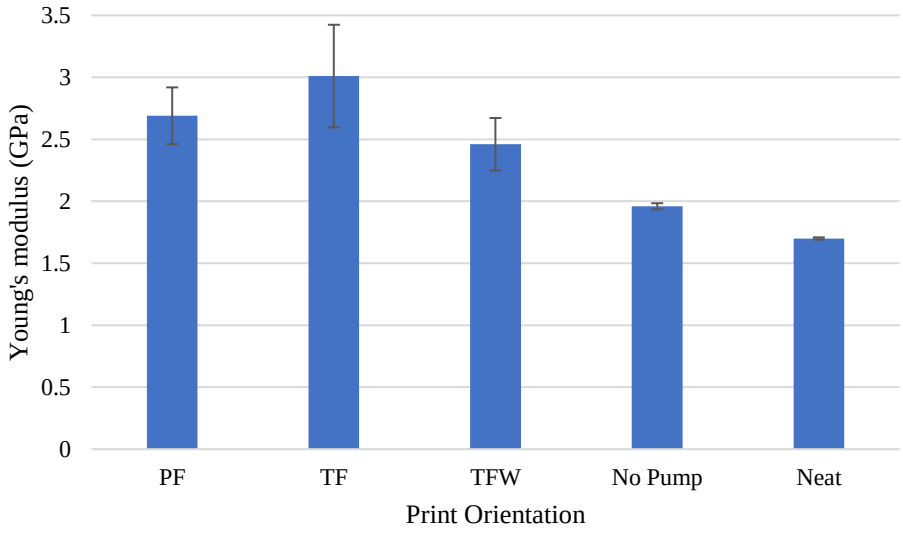

Figure 38: Average Young's modulus of samples.

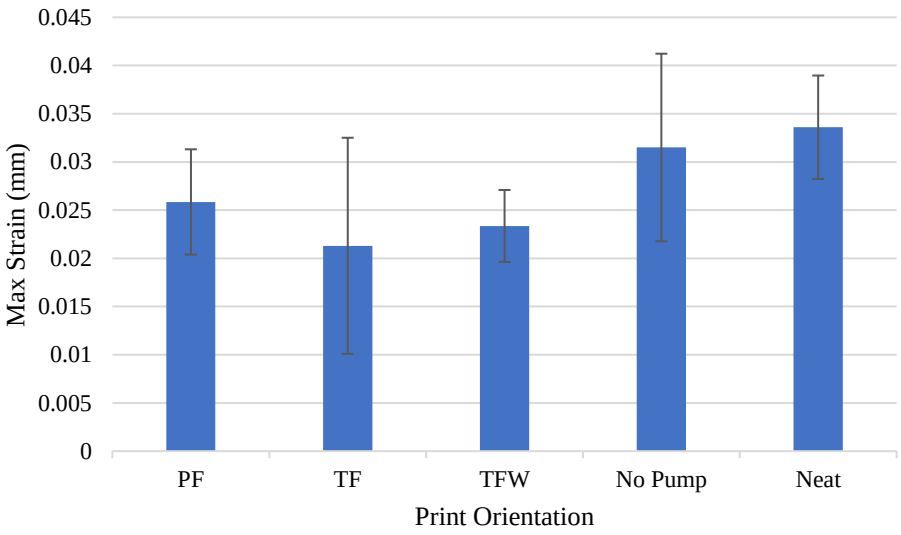

Figure 39: Average strain-to-failure samples.

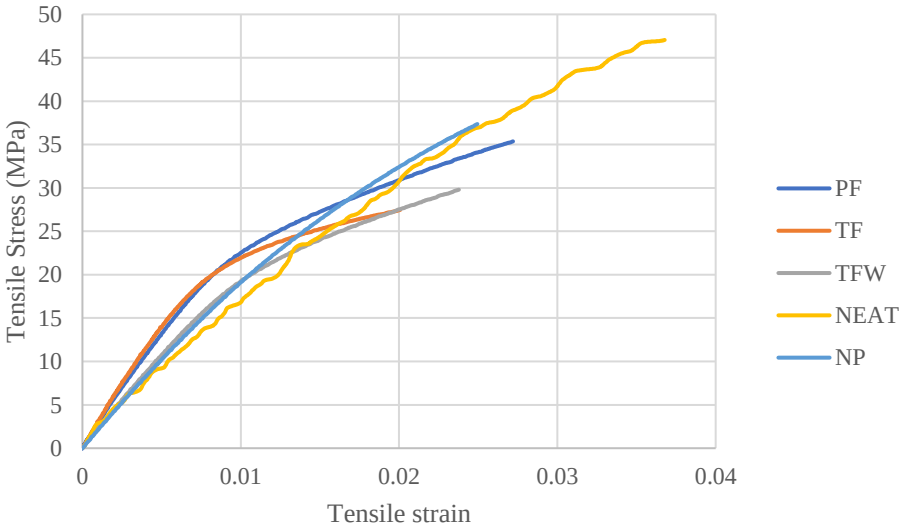

Figure 40: Stress vs. strain curves for averages of printed samples.

After the tensile testing was completed, adding the glass fiber was found to have a significant impact on Young's modulus increasing it on an average of 59.4%. The highest increase of the three print orientations was observed with the TF orientation with a 77% increase. During the elastic regime of the stress vs. strain curve, the glass fibers restricted the polymer chain motion, therefore increasing the Young's modulus. It was also observed that there was a

poor interface between the fibers and resin matrix, this will be further explained later in the thesis. There is a clear elastic region and plastic region for all samples that had at least some glass present. The tensile strength decreased for all orientation on an average of 30% with the lowest being 20.9% in print orientation PF. Strain-to-failure in all print orientations decreased, on average the decrease was 30%, with a max decrease of 37%. These decrease will later be explained when evaluating the SEM images. As the Young's modulus increased it was expected the strain-to-failure would decrease. This is also caused by the limitation of polymer chain motion. These tests concluded that the pumping system helped to suspend the fibers in the UV resin and allowed for a more uniform distribution of the glass fibers in the composite. No further testing of the no pump resin was examined. The reasoning behind this decision was a clear increase in Young's modulus was observed and the results from the gradient and density testing.

6.6. Flexural Testing

Flexural testing was completed to observe how each specimen would fracture and to examine the different mechanical properties such as max flexure stress and modulus. The results of this test would also reveal tensile compression and shear properties. The samples were all printed in the PF orientation. This was done because properties found in the tensile testing had a lower standard deviation. Samples were printed to a 16:1 ratio. The graphs for max flexure stress, modulus, and max strain for the neat samples can be seen in the Appendix under A.21, A.22, and A29. The stress vs. strain curve can be seen in the Appendix A.37.

Glass fiber reinforced samples were then printed and tested to examine the change in the max flexure stress, modulus, and max strain. The samples were printed three at a time and sanded similar to that of tensile samples. The graphs for max flexure stress, modulus, and max strain for the glass fiber reinforced samples can be seen in the Appendix under A.23, A.24, and

A.30. The flexure stress vs. strain curve can be seen in Appendix A.38. The max flexure stress and modulus of both the neat and 15% by volume reinforced samples were then compared to each other. These graphs can be seen below in Figure 41. The average stress vs. strain curve can be seen in Figure 42.

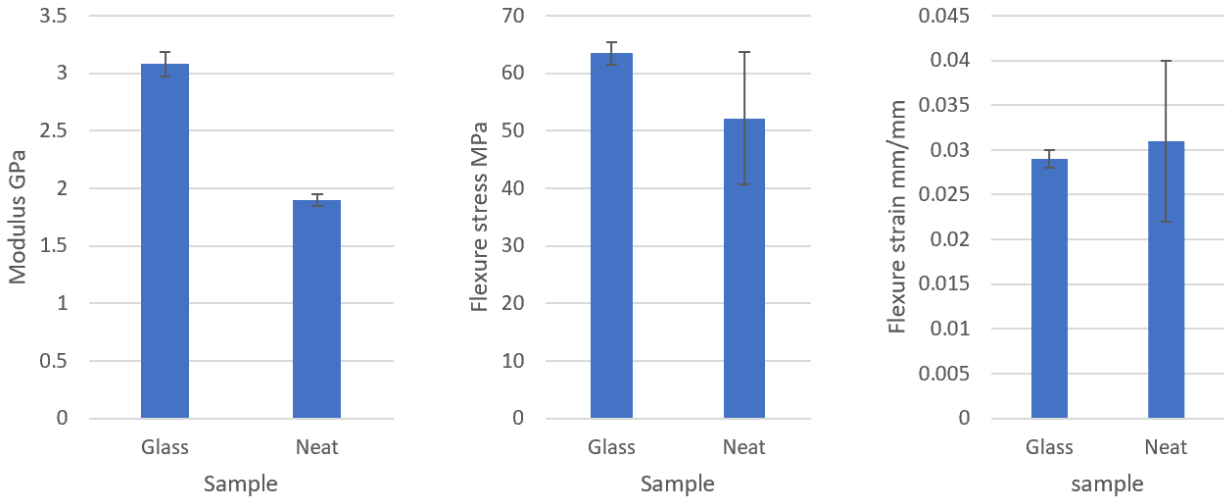

Figure 41: Comparison of neat and glass fiber reinforced samples of: modulus, flexure stress, and flexure strain.

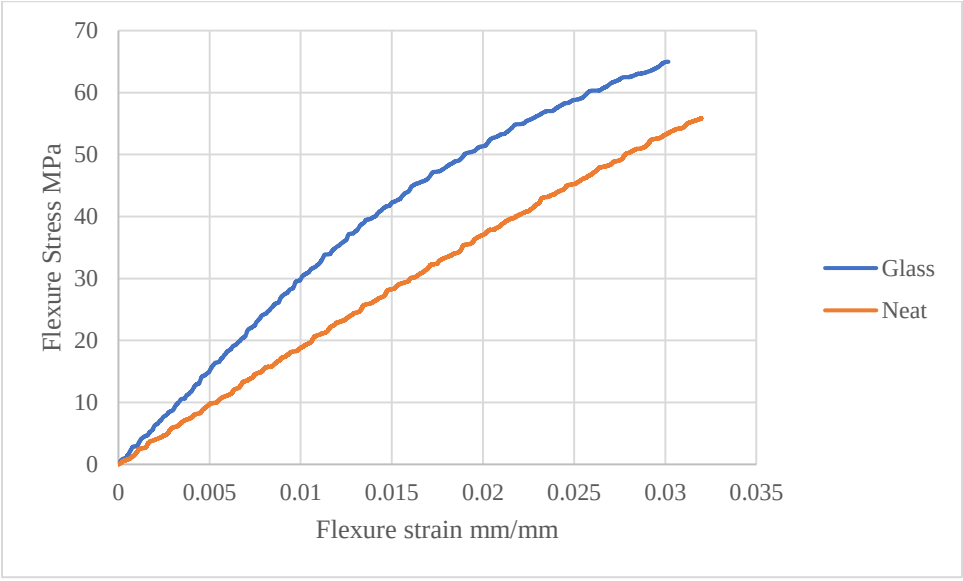

Figure 42: Stress vs. strain curve of neat and glass fiber reinforced samples.

The addition of the glass fiber increased the flexure stress by 18%, increase the modulus of 38% and decrease the max strain by .002%. The flexure samples were printed with a 16:1

ratio of length to thickness but still had to be designed small enough to fit in the printing surface. Larger samples would be desired to find better max flexure stress and modulus, this is due to the increase in the bending moment. The fracture type was different between neat and glass fiber reinforced samples. The neat samples broke into multiple different pieces where the reinforced samples had a single fracture. The addition of the glass fibers helped to dampen the vibration of the free-falling piece therefore limiting to only one fracture and not multiple [39].

6.7. Notch Fracture Toughness K_{IC}

The samples tested for fracture toughness were also printed in the PF orientation. The samples were examined under a Keyence VHX-7000 Digital Microscope. A photo of this microscope can be seen below in Figure 42.

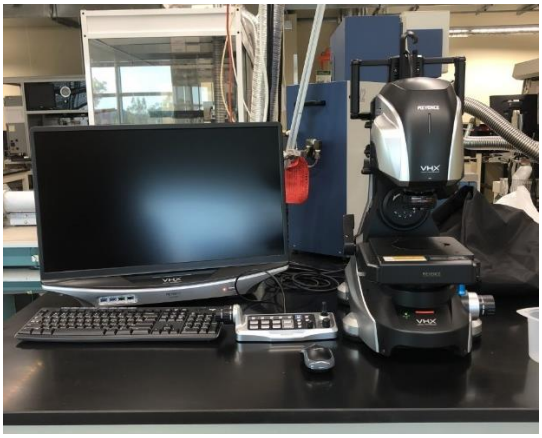

Figure 43: Keyence VHX-7000 Digital Microscope.

This microscope was used to measure the crack length in each sample for the calculation of fracture toughness from each test. A calibration factor was then calculated, this factor ensured that each specimen where comparable and is This donated as $f(x)$. This factor takes in to account the geometry of each specimen. Starting this process began with finding the crack length. Using the microscope above the crack length *a* could be found and a ratio of crack length and width was calculated. This can be seen below in equation 6.6.

$$x = \frac{a}{w} \tag{6.6}$$

The ratio shown has *a* "crack length" and *w* "width" of the sample. This ratio was then used to find *f(x).* This equation can be seen below.

$$f(x) = 6x^{1/2}\frac{[1.99 - x(1-x)(2.15 - 3.93x + 2.7x^2)]}{(1+2x)(1-x)^{3/2}} \tag{6.7}$$

Once this *f(x)* was calculated the fracture toughness K_{IC} could be found using the equation shown below.

$$K_{IC} = \left(\frac{P_Q}{BW^{\frac{1}{2}}}\right) f(x) \tag{6.8}$$

In this equation K_{IC} is the fracture toughness, P_Q is the max flexure load, *B* is the thickness at the crack, and *W* is the width at the crack. A 32.5% increase in fracture toughness can be observed when adding 15% glass fiber to the sample. Stress vs. strain curves of the neat and glass reinforced samples can be seen in Appendix A.39 and A.40. These results can be seen below in Figure 44 and a comparison of the stress vs. strain curves can be seen in Figure 45.

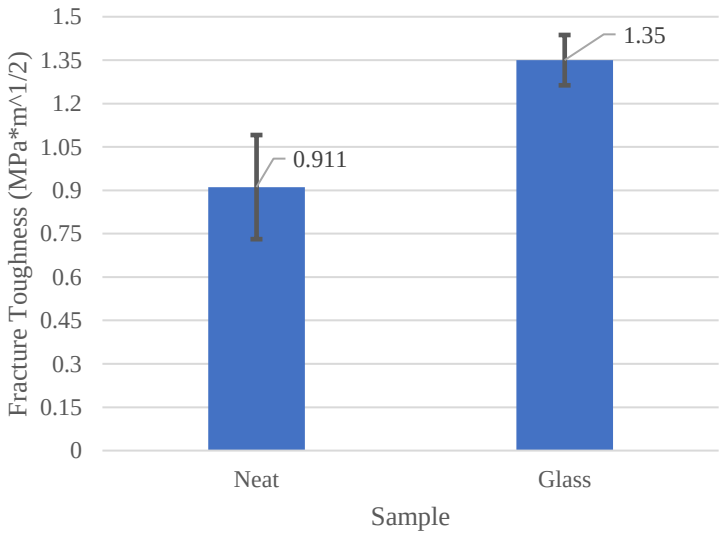

Figure 44: Average fracture toughness of both neat and glass reinforced samples.

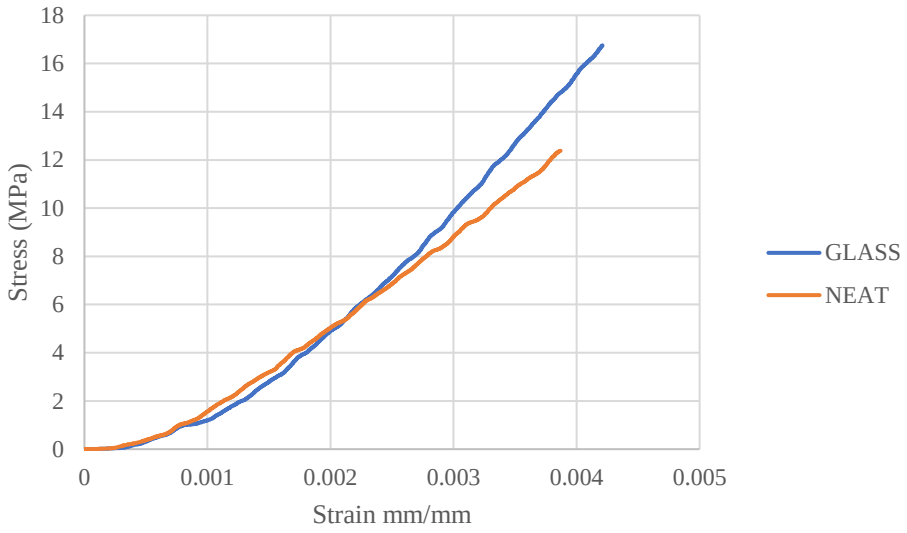

Figure 45: Stress vs. strain curve comparing neat and glass reinforced samples.

6.8. Scanning Electron Microscope Images

A baseline of the neat resin had to be scanned first to compare the glass fiber reinforced composite. The neat resin was scanned to examine the quality of the prints and determine if the neat resin had voids. Figure 46 shows an image of the fracture surface from fracture testing.

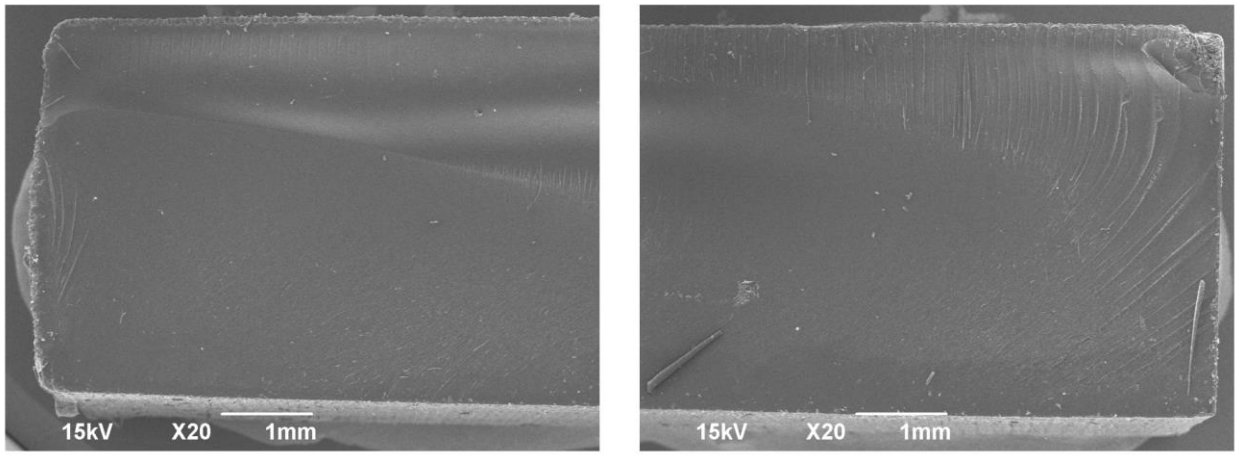

Figure 46: Total fracture surface of a neat flexure sample.

When examining the neat resin, there were no void spots and no porosity along the entire fracture surface in comparison to earlier studies showing there would be voids spots and porosity with the addition of carbon fiber [6]. The glass fiber tensile samples were then taken and

examined with the SEM. The picture below on the left shows the longitudinal axis of the samples to view for fiber orientation and fiber pullout. The picture on the right is a view of the fracture surface. These images can be seen below in Figure 47 and Figure 48.

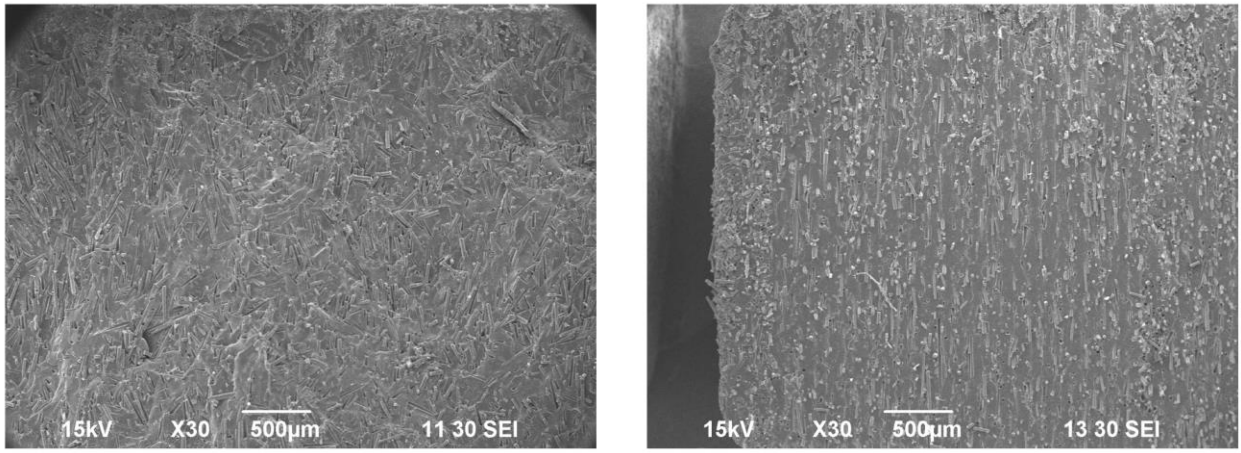

Figure 47: Longitudinal surface of tensile sample and fracture surface of glass reinforced tensile sample.

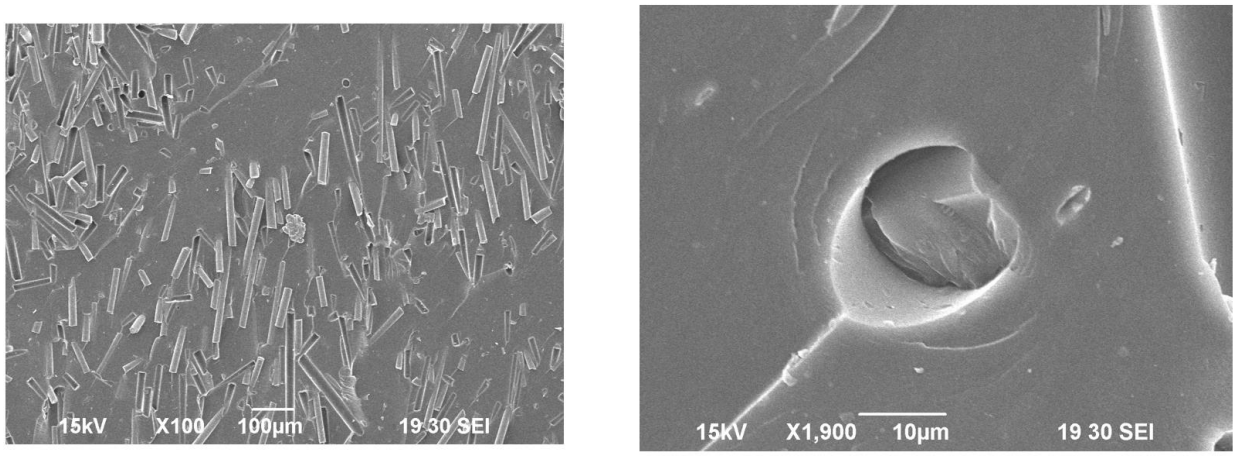

Figure 48: Fracture surface of glass reinforced tensile samples and expanded view of fiber breakage.

After tensile testing was complete a gauge section of the sample was split in half using a blade and hammer. In Figure 48 the image on left shows the fibers are randomly orientated. The image also shows both fiber pull out and fiber breakage. These finding can explain why there was a decrease in the tensile strength. The pullout from the resin of the fibers show a poor

interface between the UV resin and the glass fibers. The SEM images also show some areas of fiber aligned in the transverse direction of the force. When this happens the glass fibers can act as a void, also lowing the tensile strength in the samples. The second images show the fracture surface of the gauge section. Fiber breakage was observed but the major of the fibers pulled out showing a poor interface between the two materials. When comparing the neat and glass fiber reinforced samples both show a near zero in porosity or voids.

7. CONCLUSION

The resins typically used in AM have low mechanical properties. In this study it was shown that by adding glass fiber some properties increased while other decreased. The Young's modulus increased by 59.4% with the addition of glass fibers. The fracture toughness also increased by 32.5%. The tensile strength decreased by 30%, this shows that when adding glass fiber to the UV resin it is possible to increase some but not all the mechanical strength of these composites. The strain-to-failure decreased in the tensile direction but remained the same during flexure. Again, this was from a poor interface between the fibers and the decrease in the polymer chain motion and proven while examining the SEM images. As a reaction to this the strain-to-failure would decrease. During flexure testing the neat and reinforced samples broke in different types. The reinforced samples had a single fracture as the neat samples had multiple. This shows by adding glass fibers to a polymer matrix not all properties will be increased. The Modulus found during flexure testing had an increase of 38%, an increase in flexure stress also had an increase of 18%.

The exact sizing agent used on the fibers could not be found. Knowing what agent was used could help determine if the mechanical properties observed could have been improved more. Because of this, the interface between the acrylate based resin and glass fibers may not have been optimal.

When examining the SEM pictures there is sections of semi-aligned fibers. The alignment of these fibers will greatly change the properties of the composite. When these small sections are aligned in the transverse direction of the force being applied, the small aligned sections can decrease the overall performance of the composite. While preparing the glass fiber reinforced notched samples for testing, the subtraction process was seen to be much easier. The

glass fiber reinforced samples did not chip or break while milling. A multitude of samples of neat resin had to be printed as 45% of neat samples broke or chipped while milling.

The addition of glass fibers increased the viscosity by nearly 50%. This could potentially cause a problem for 3D printers that rely on a lower viscosity. Other concerns arise with the pump system explained in this research. If the hosing used is too small the resin and glass fiber could make it difficult for the motor to pump the needed amount of resin through the inlet, to ensure a flow field.

Lastly, when using this pump system, a large amount of resin is wasted after each print. If a new mixture is not made before each print the true fiber volume will not be known. In the corners and along the far edges of the resin tank the glass fibers settle. Remixing the remaining resin and glass fiber may not be what was originally made. In conclusion, the addition of glass fibers to a UV resin matrix increases mechanical properties such as Young's modulus and fracture toughness and has no effect or decrease in tensile strength, max fracture stress, and modulus.

8. RECOMMENDATIONS

Glass fiber was chosen because it is transparent to UV light. With added length, more of the force can be transferred to the fibers. If longer fibers were introduced the pumping system would have to be reevaluated to accommodate this. Different sizing agents should be investigated. Improving the interface between the glass fibers and the resin matrix would improve fiber pull out, this would then allow for more of the force to be absorbed by the fibers and not the polymer matrix. Larger inlet, outlet, and hosing would have to be used and a larger pump that could produce a higher flow rate should also be investigated. The Moai printer has the ability to change the layer thickness. Changing the thickness should also be investigated to determine if a larger or small print layer could change the mechanical properties or distribution of fibers. If new fibers are to be used, the Stoke equations should be considered when determining a new flow rate. The streamlines of the UV resin and glass fibers became more constant as the velocity of the fluid increased. Further work should investigate these findings.

REFERENCES

[1] Hull, C. W., 1986, "Apparatus for production of three-dimensional objects by stereolithography," U.S. Patent 4575330A

[2] 3D Printer PLA Filament. (n.d.). Retrieved from https://gizmodorks.com/pla-3d-printer-filament/

[3] Source, F. P. (n.d.). Polymer Properties Database. Retrieved from https://polymerdatabase.com/polymer classes/UV Curing Resins.html#:~:text=Typical UV curable resins consist,antioxidants, plasticizers, and pigments.

[4] FDM (3D Printing) – Simply Explained. (2020, March 05). Retrieved from https://all3dp.com/2/fused-deposition-modeling-fdm-3d-printing-simply-explained/

[5] Jacobs, P. F., Rapid Prototyping & Manufacturing: Fundamentals of Stereolithography, Society of Manufacturing Engineers, (1992)

[6] Simpson, Patrick Glenn. 2018

[7] Mendes-Felipe, C., Oliveira, J., Etxebaaria, I., & Vilas-Vilela, J. (2019). State-of-the-Art and Future Challenges of UV Curable Polymer-Based Smart Materials for Printing Technologies. *Advanced Materials Technologies, 4*(3).

[8] Rajak, D. K., Pagar, D. D., Menezes, P. L., & Linul, E. (2019, October 12). Fiber-Reinforced Polymer Composites: Manufacturing, Properties, and Applications. Retrieved from https://www.ncbi.nlm.nih.gov/pmc/articles/PMC6835861/

[9] The Ultimate Guide to Stereolithography (SLA) 3D Printing (Updated for 2020). (n.d.).Retrieved from https://formlabs.com/blog/ultimate-guide-to-stereolithography-sla-3d-printing/#A Brief History of Stereolithography

[10] DLS 3D Printing Technology: Carbon. (2020, September 18). Retrieved from https://www.carbon3d.com/3d-printer-models-carbon/our-technology/

[11] Masere, J., Chekanov, Y., Warren, J. R., Stewart, F. D., Al-Kaysi, R., Rasmussen, J. K., and Pojman, J. A. "Gas-free initiators for high-temperature free-radical polymerization," *Journal of Polymer Science Part A: Polymer Chemistry*, Vol. 38 No. 21 (2000): pp. 3984-3990.

[12] Sano, Y., Matsuzaki, R., Ueda, M., Todoroki, A., & Hirano, Y. (2018). 3D printing of discontinuous and continuous fibre composites using stereolithography. *Additive Manufacturing, 24*, 521-527. Retrieved October 8, 2020.

[13] Blok, L.G., et al. “An Investigation into 3D Printing of Fibre Reinforced Thermoplastic Composites.” *Additive Manufacturing*, Elsevier, 1 May 2018, www.sciencedirect.com/science/article/pii/S2214860417305687

[14] Serope Kalpakjian, Steven R Schmid. "Manufacturing Engineering and Technology". International edition. 4th Ed. Prentice Hall, Inc. 2001.

[15] Advani, S. G. (2012). *Manufacturing techniques for polymer matrix composites (PMCs)*. Oxford: Woodhead Publishing.

[16] Arnaut, K., Schiebel, P., Lang, A., & Herrmann, A. S. (2015). Reinforcement elements aligned with the direction of forces for load transfer areas of long-fiber-reinforced thermoplastic components. *Materials Science Forum, 825-826*, 779-786.

[17] "Creep behavior of carbon fiber/epoxy matrix composites," *Materials Science and Engineering*. 13-Dec-2005

[18] Wang, X., Zhao, X., Chen, S., & Wu, Z. (2020). Static and fatigue behavior of basalt fiber-reinforced thermoplastic epoxy composites. *Journal of Composite Materials, 54*(18), 2389–2398. https://doi.org/10.1177/0021998319896842

[19] Benefits of Long Fiber Reinforced Thermoplastic Composites. (2019, August 12). Retrieved from https://www.plasticomp.com/long-fiber-benefits/

[20] Solution for Carbon fiber Wet-Out Issue for Low Cost Sheet ... (n.d.). Retrieved from https://www.ornl.gov/sites/default/files/2019-06/web_Continental-Structural-Plastics-Report.pdf

[21] Akil, H., Omar, M., Mazuki, A., Safiee, S., Ishak, Z., & Bakar, A. A. (2011). Kenaf fiber reinforced composites: A review. *Materials & Design, 32*(8-9), 4107-4121. doi:10.1016/j.matdes.2011.04.008

[22] Boosting Performance without Breaking the Bank. (2019, June 14). Retrieved from https://www.assemblymag.com/articles/94868-boosting-performance-without-breaking-the-bank

[23] Kahl, C., Feldmann, M., Sälzer, P., & Heim, H. (2018). Advanced short fiber composites with hybrid reinforcement and selective fiber-matrix-adhesion based on polypropylene – Characterization of mechanical properties and fiber orientation using high-resolution X-ray tomography. *Composites Part A: Applied Science and Manufacturing, 111*, 54-61. doi:10.1016/j.compositesa.2018.05.014

[24] Agarwal, B. D., Broutman, L. J., & Chandrashekhara, K. (2018). *Analysis and performance of fiber composites*. Hoboken, NJ: Wiley.

[25] (2014). Army Research Laboratory S&T Campaign Plans 2015-2035. 8 October 2020 Retrieved from https://www.hsdl.org/?abstract&did=762115

[26] Sackey, Samuel S., et al. "Spectroscopic Study of UV Transparency of Some Materials." *Environment and Pollution*, vol. 4, no. 4, 2015, doi:10.5539/ep.v4n4p1.

[27] “15 Different Types of Fiberglass.” *Home Stratosphere*, 19 Dec. 2019, www.homestratosphere.com/types-of-fiberglass/.

[28] VWR Laboratory Vacuum Oven 1415M: ANDbio. (2020, September 15). Retrieved from https://www.andbio.com/shop/3363235-vwr-laboratory-vacuum-oven-1415m/#/

[29] Moai 130 SLA printer - Assembled version. (n.d.). Retrieved from https://peopoly.net/products/moai-130-sla-printer-kit

[30] Similar To High Flow Peristaltic Pump DC. (n.d.). Retrieved from https://gistgear.com/product/B07R7K8R5K

[31] 1/32 Inch Milled Glass Fibers. (n.d.). Retrieved from https://www.fibreglast.com/product/132_inch_Milled_Glass_Fibers_38

[32] Thomason, J. (2019). Glass fibre sizing: A review. *Composites Part A: Applied Science and Manufacturing, 127*, 105619. doi:10.1016/j.compositesa.2019.105619

[33] ASTM D5418-15 Standard Test Method for Plastics: Dynamic Mechanical Properties: In Flexure (Dual Cantilever Beam), ASTM International, West Conshohocken, PA, 2015

[34] ASTM D638-14 Standard Test Method for Tensile Properties of Plastics, ASTM International, West Conshohocken, PA, 2014

[35] ASTM D3039/D3039M-17 Standard Test Method for Tensile Properties of Polymer Matrix Composite Materials, ASTM International, West Conshohocken, PA, 2017

[36] ASTM D790-17 Standard Test Methods for Flexural Properties of Unreinforced and Reinforced Plastics and Electrical Insulating Materials, ASTM International, West Conshohocken, PA, 2017

[37] ASTM D5045-14 Standard Test Methods for Plane-Strain Fracture Toughness and Strain Energy Release Rate of Plastic Materials, ASTM International, West Conshohocken, PA, 2014

[38] Agarwal, B. D., Broutman, L. J., and Chandrashekhara, K. *Analysis and Performance of Fiber Composites*, John Wiley & Sons, New York (2017).

[39] Audoly, B., & Neukirch, S. (2005). Fragmentation of Rods by Cascading Cracks: Why Spaghetti Does Not Break in Half. *Physical Review Letters, 95*(9). doi:10.1103/physrevlett.95.095505

APPENDIX. SUPPLEMENTAL FIGURES

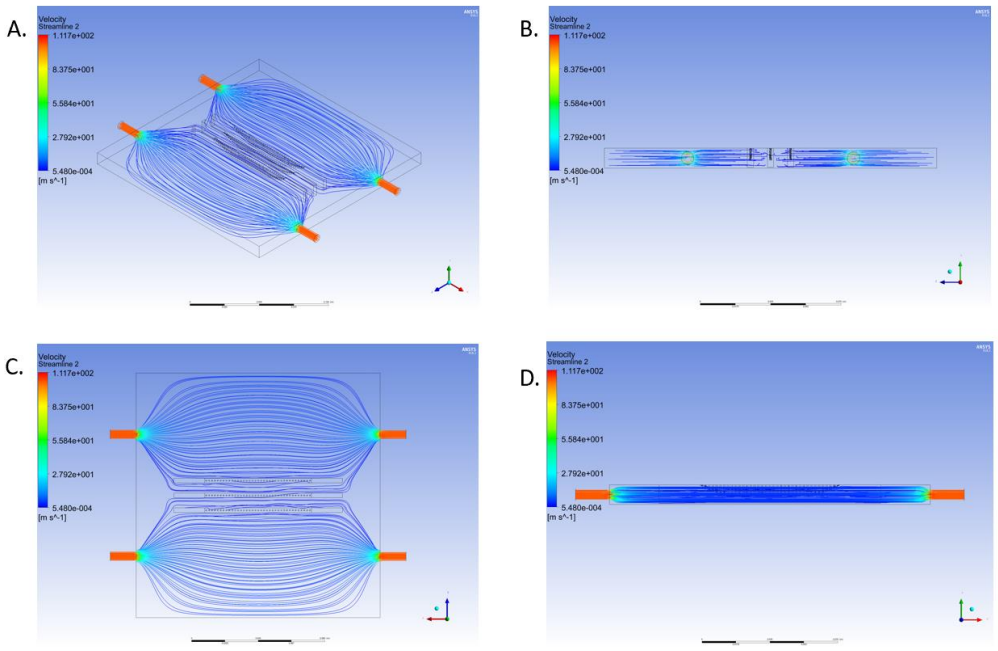

Figure A.1: CFD of tensile sample parallel to the flow at 100 µm from the bottom of resin tank bed.

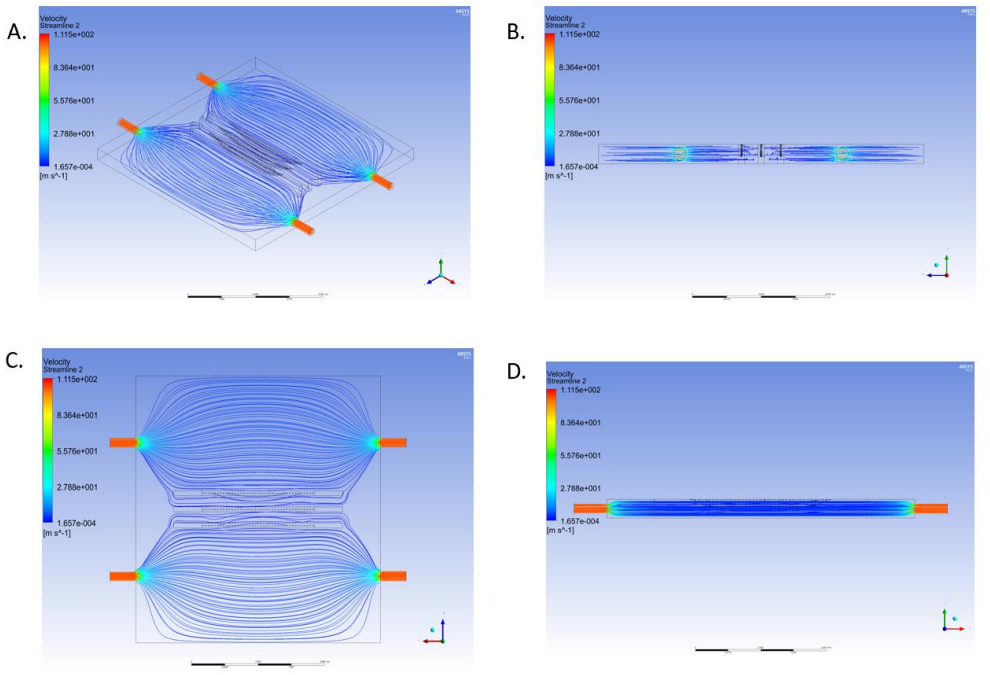

Figure A.2: CFD of tensile sample parallel to the flow at 0 µm from the bottom of resin tank bed.

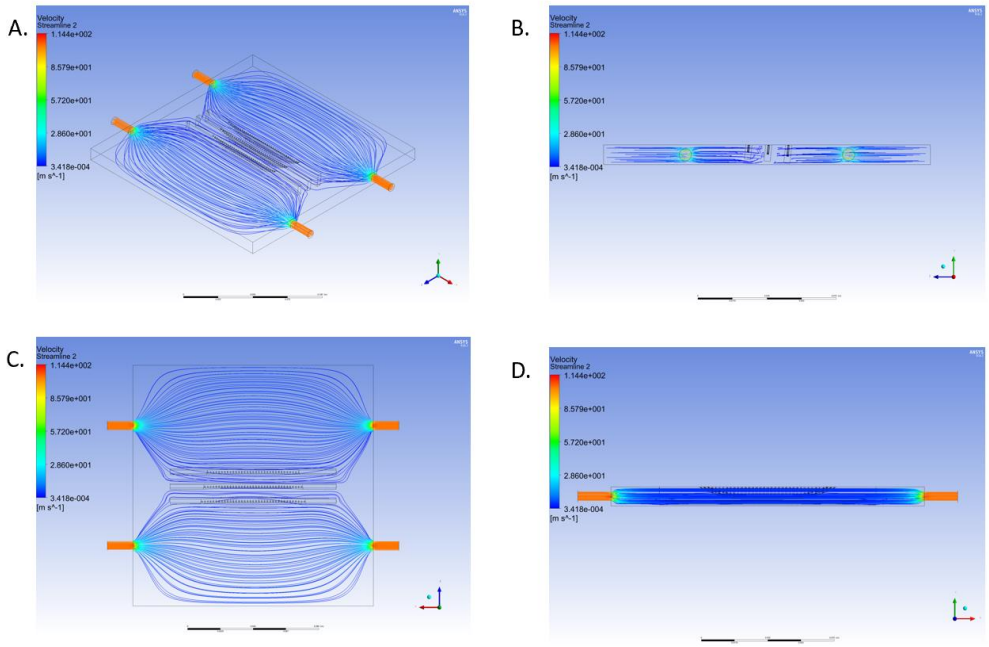

Figure A.3: CFD of tensile sample parallel to the flow at highest peel step angle.

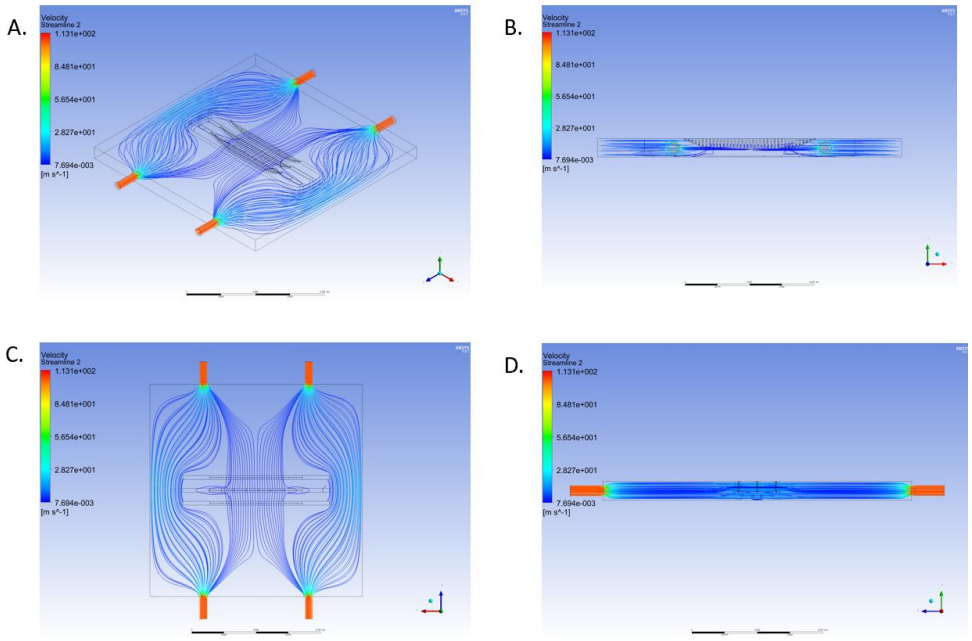

Figure A.4: CFD of tensile sample transverse to the flow at 100 µm from the bottom of resin tank bed.

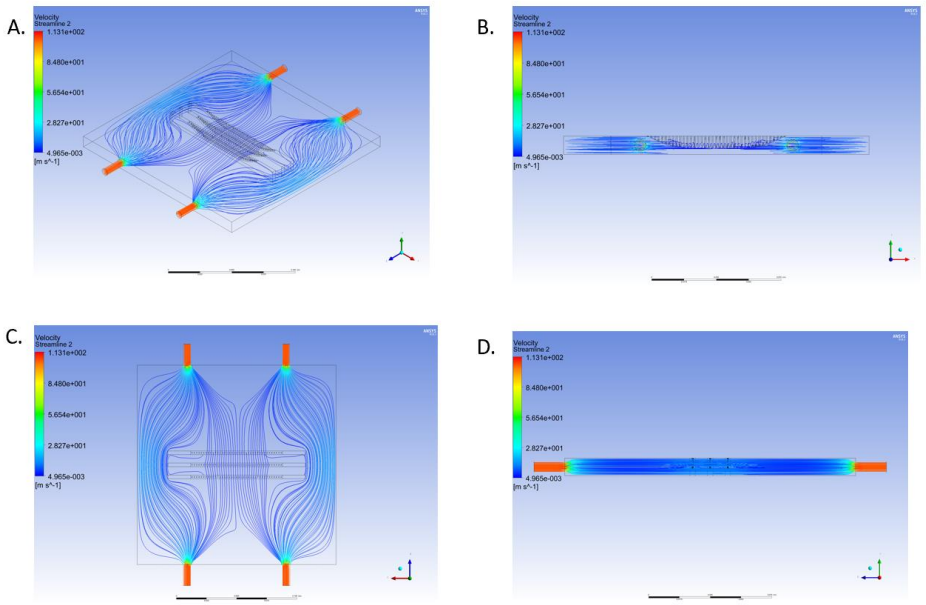

Figure A.5: CFD of tensile sample transverse to the flow at 0 µm from the bottom of resin tank bed.

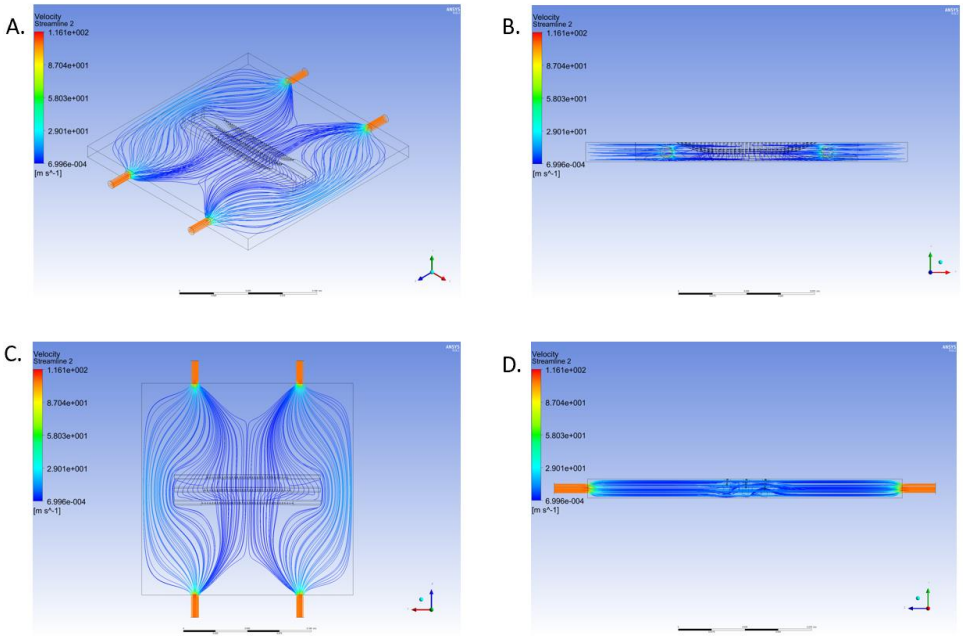

Figure A.6: CFD of tensile sample transverse to the flow at highest peel step angle.

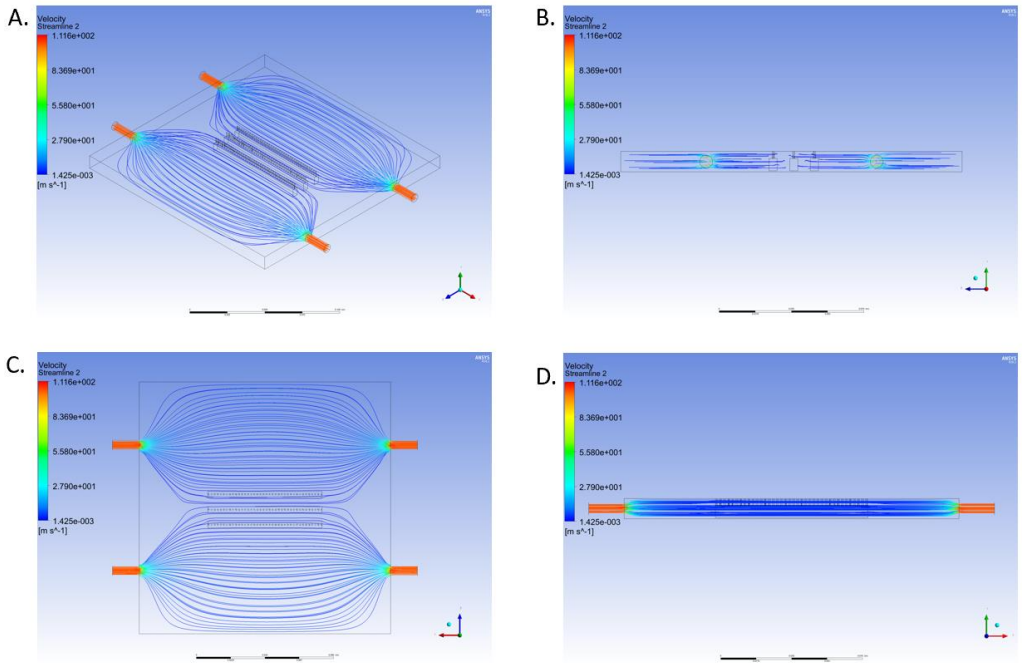

Figure A.7: CFD of flexure sample parallel to the flow at 100 µm from the bottom of resin tank bed.

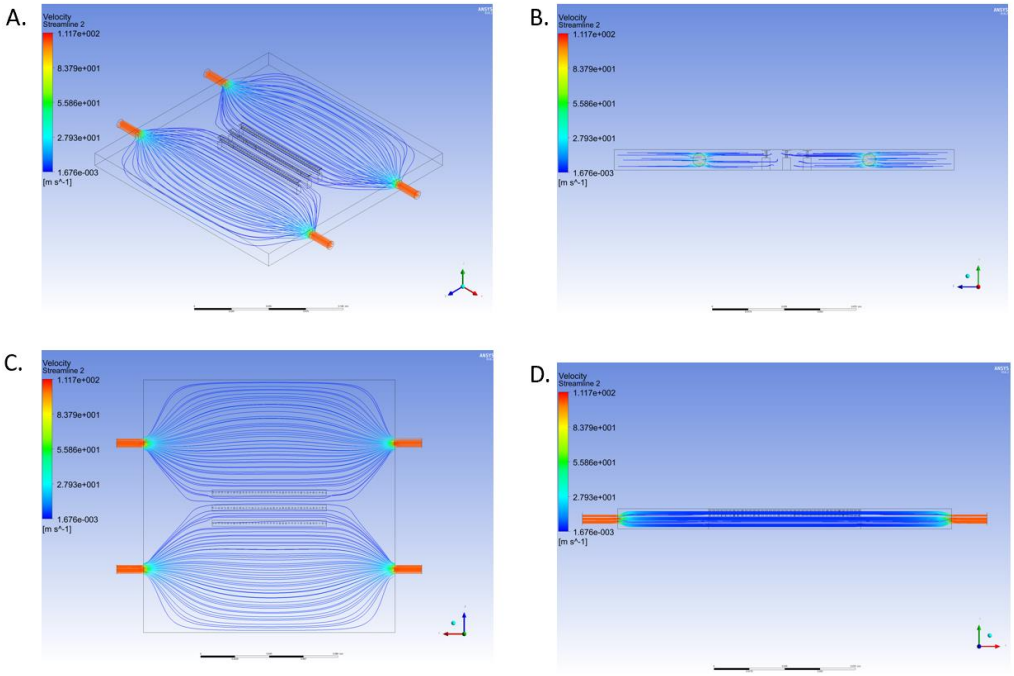

Figure A.8: CFD of flexure sample parallel to the flow at 0 µm from the bottom of resin tank bed.

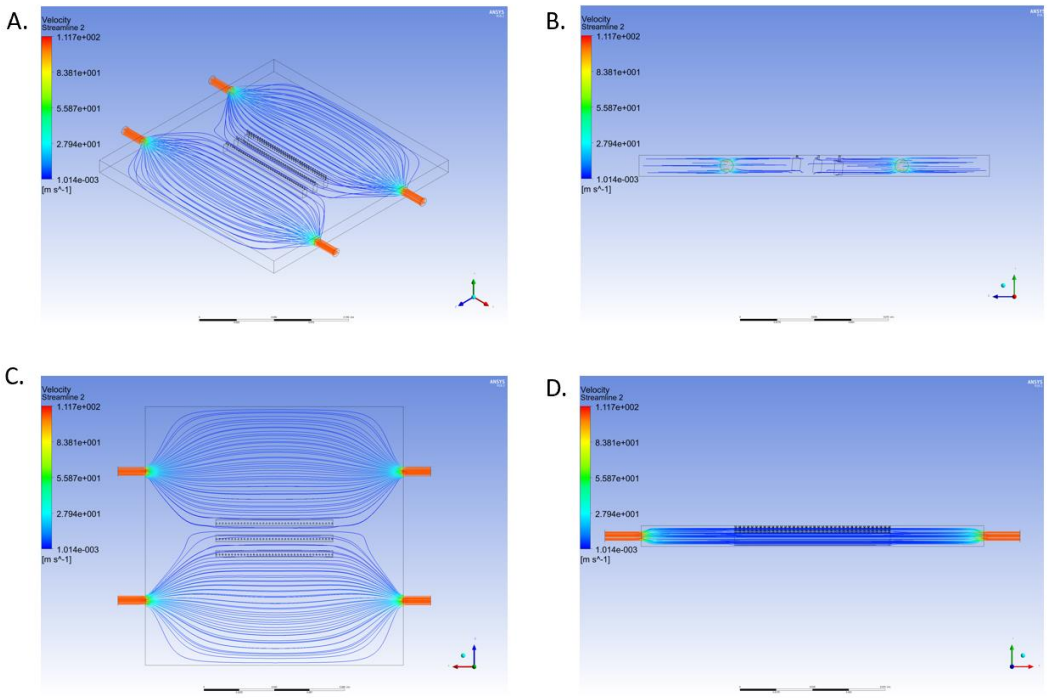

Figure A.9: CFD of flexure sample parallel to the flow at highest peel step angle.

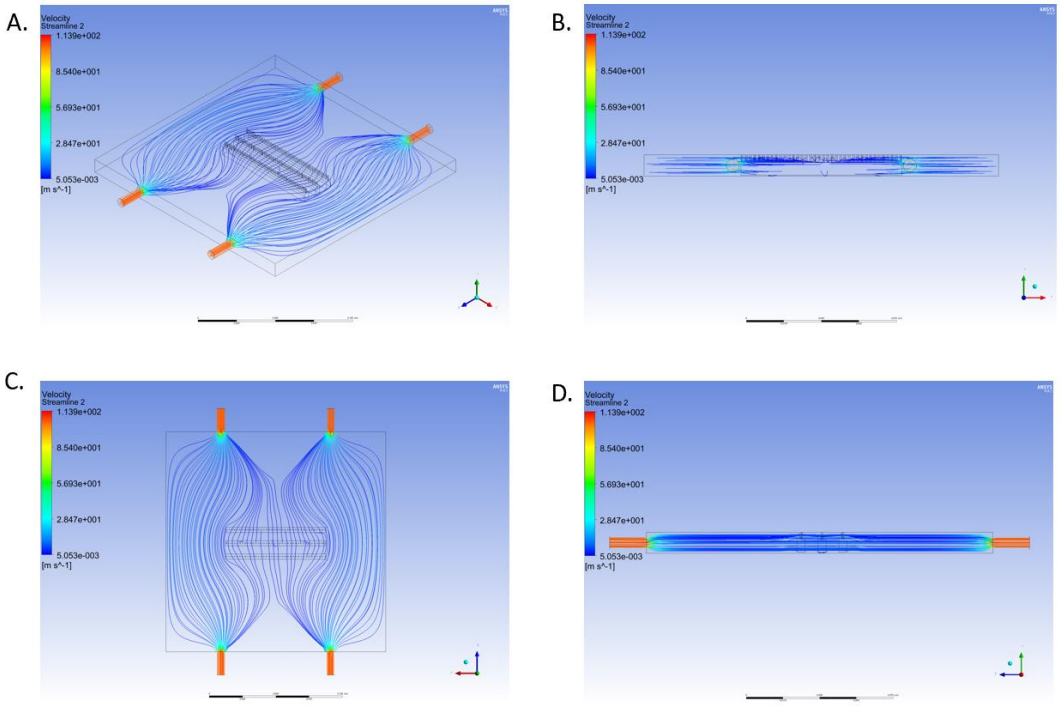

Figure A.10: CFD of flexure sample transverse to the flow at 100 µm from the bottom of resin tank bed.

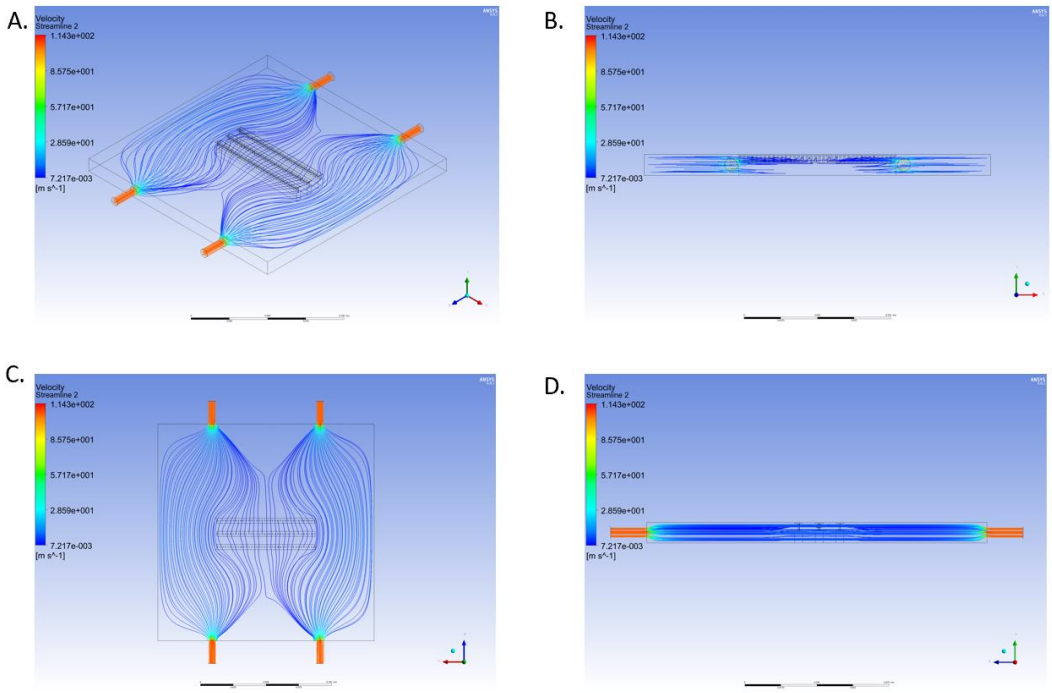

Figure A.11: CFD of flexure sample transverse to the flow at 0 µm from the bottom of resin tank bed.

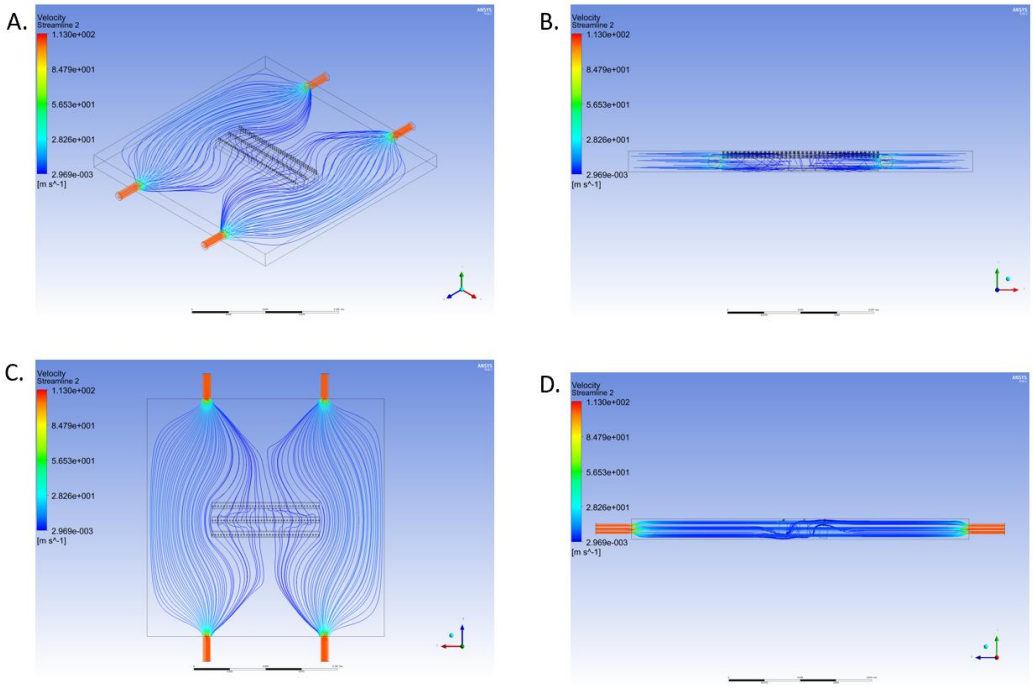

Figure A.12: CFD of flexure sample transverse to the flow at highest peel step angle.

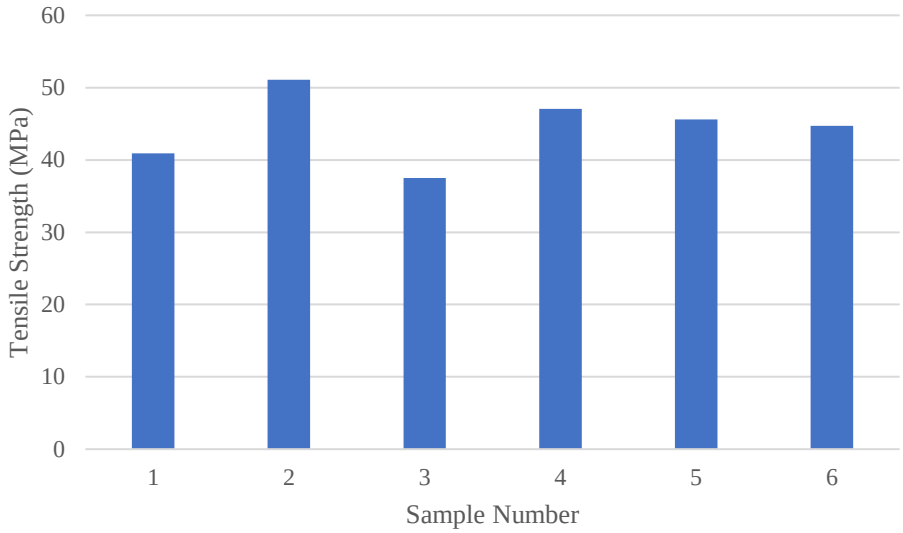

Figure A.13: Tensile strength of neat resin samples.

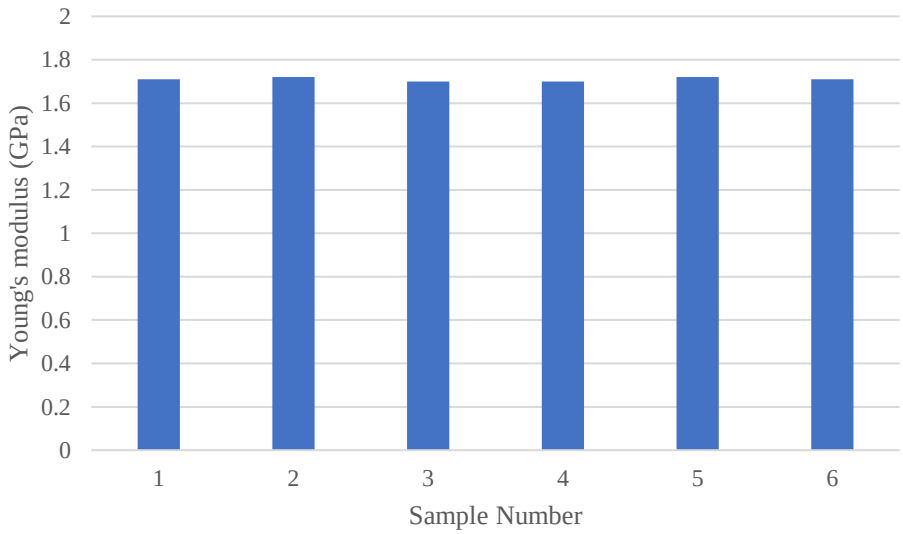

Figure A.14: Young's modulus of neat resin samples.

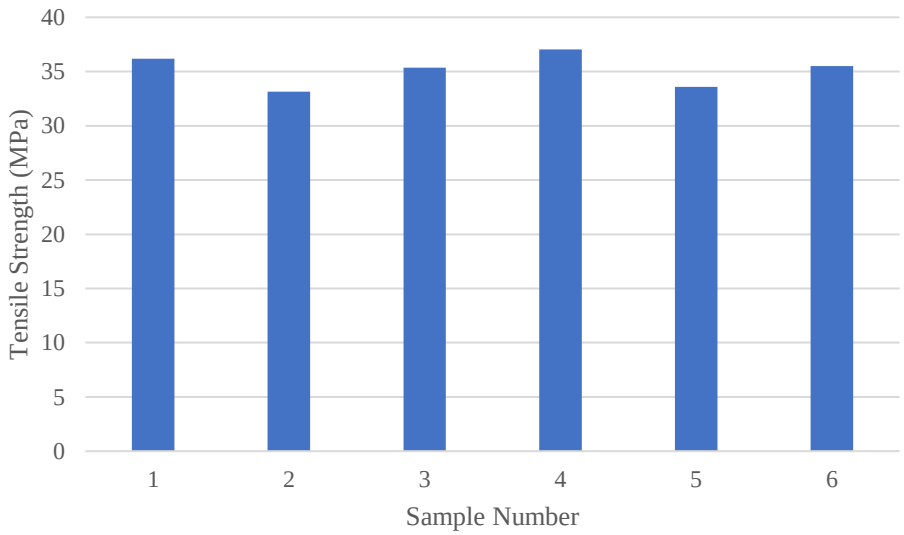

Figure A.15: Tensile strength of resin and 15% by volume glass fibers in PF print orientation.

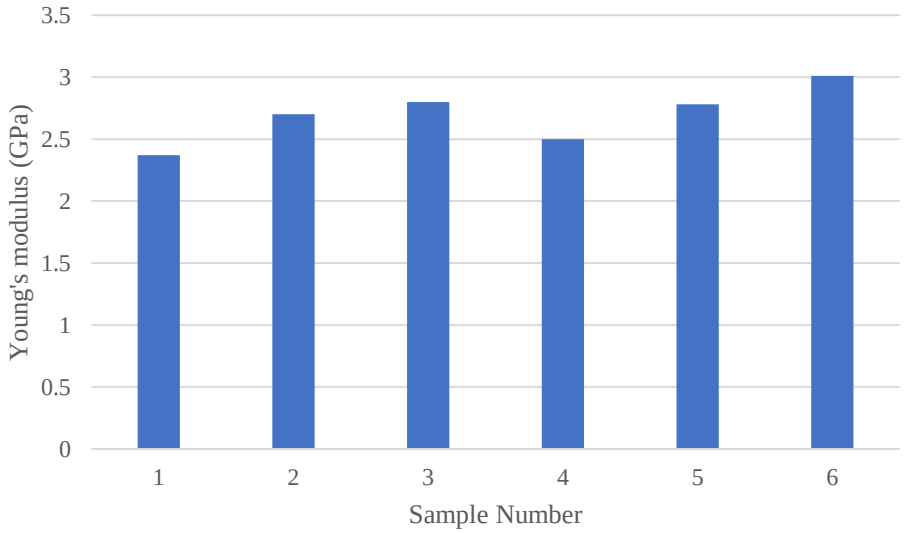

Figure A.16: Young's modulus of resin and 15% by volume glass fibers in PF print orientation.

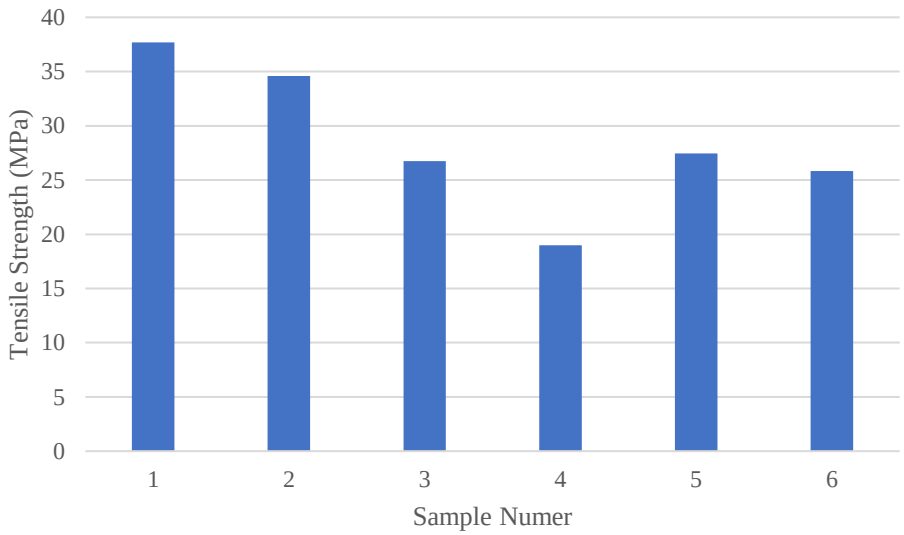

Figure A.17: Tensile strength of resin and 15% by volume glass fibers in TF print orientation.

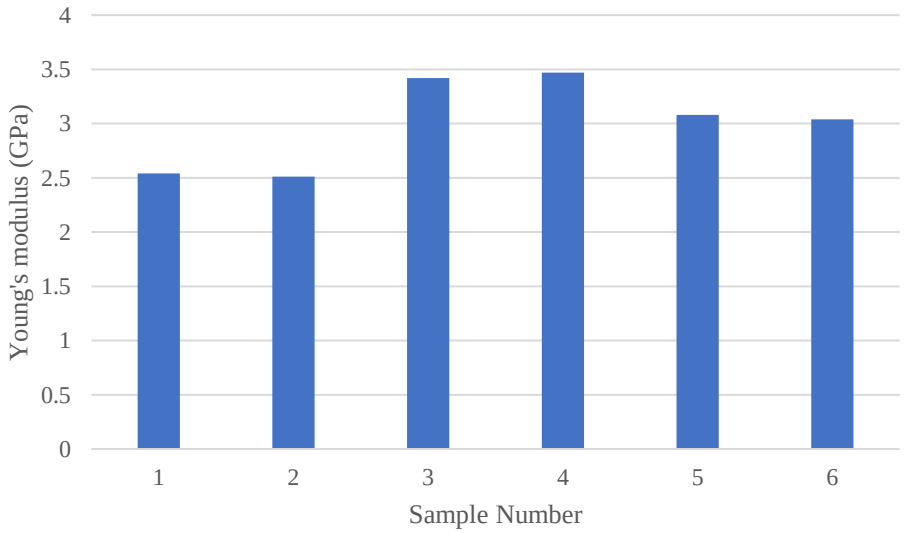

Figure A.18: Young's modulus of resin and 15% by volume glass fibers in TF print orientation.

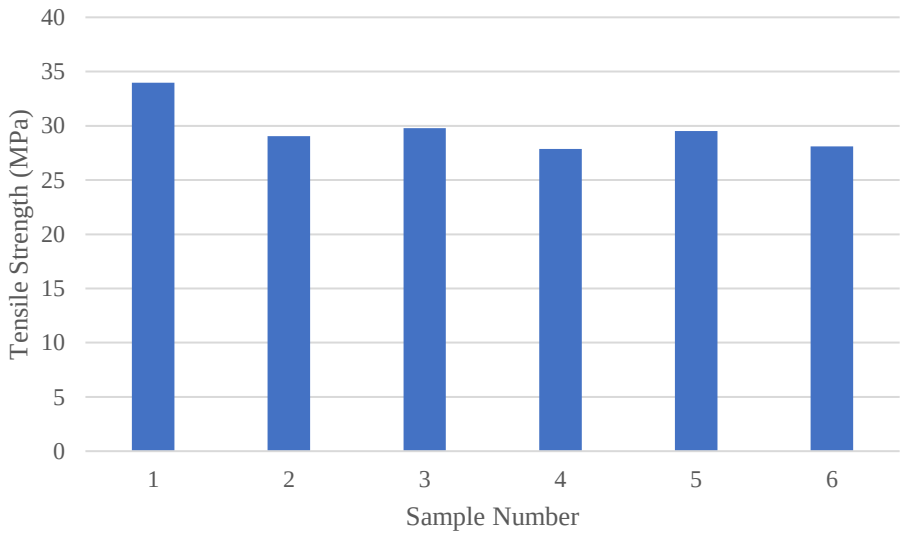

Figure A.19: Tensile strength of resin and 15% by volume glass fibers in TFW print orientation.

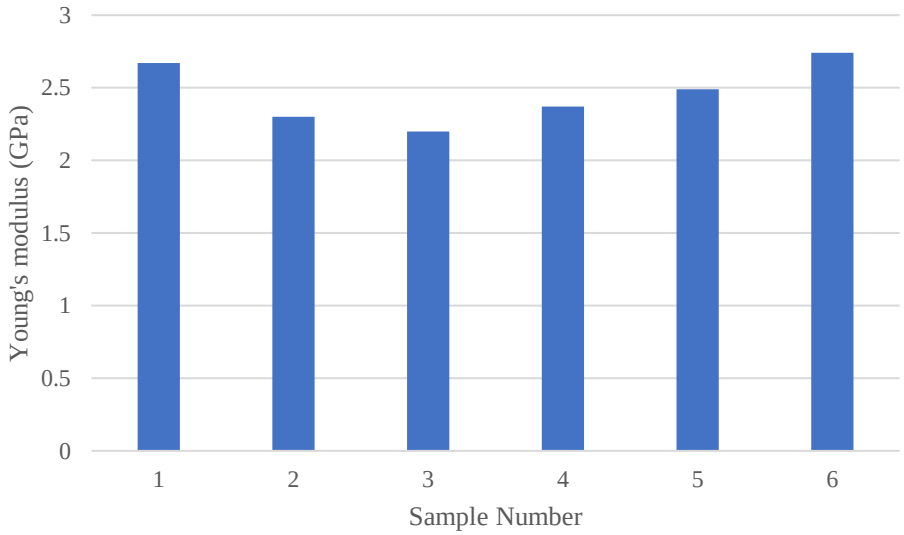

Figure A.20: Young's modulus of resin and 15% by volume glass fibers in TFW print orientation.

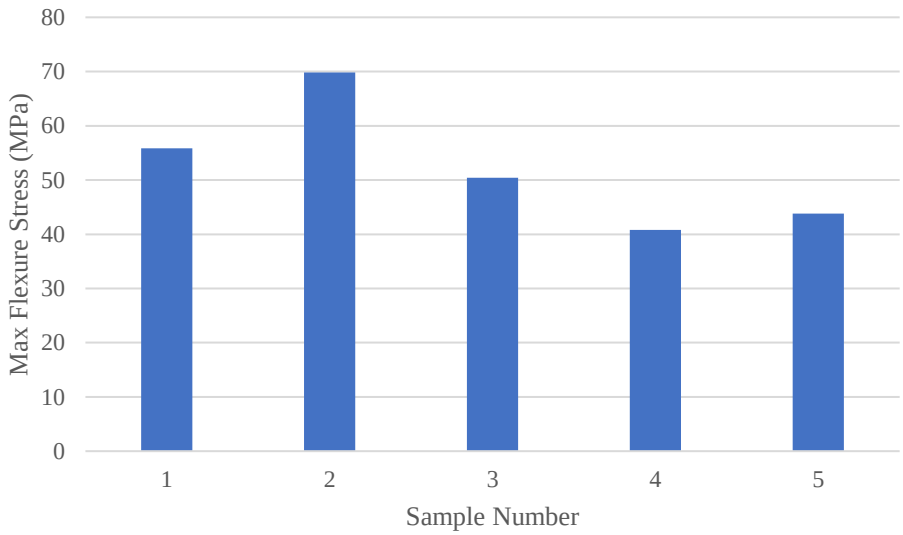

Figure A.21: Max flexure stress of neat resin.

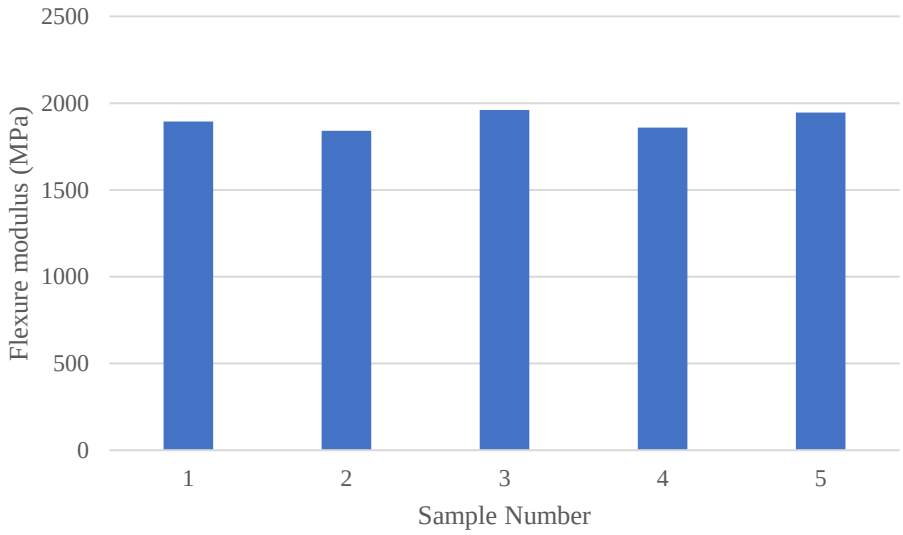

Figure A.22: Flexure modulus of neat resin.

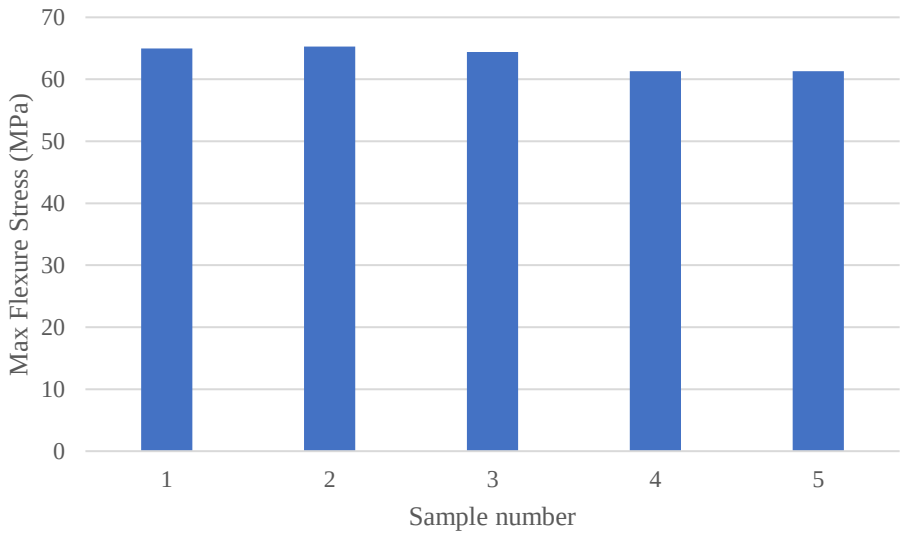

Figure A.23: Max flexure stress of resin and 15% by volume glass fibers.

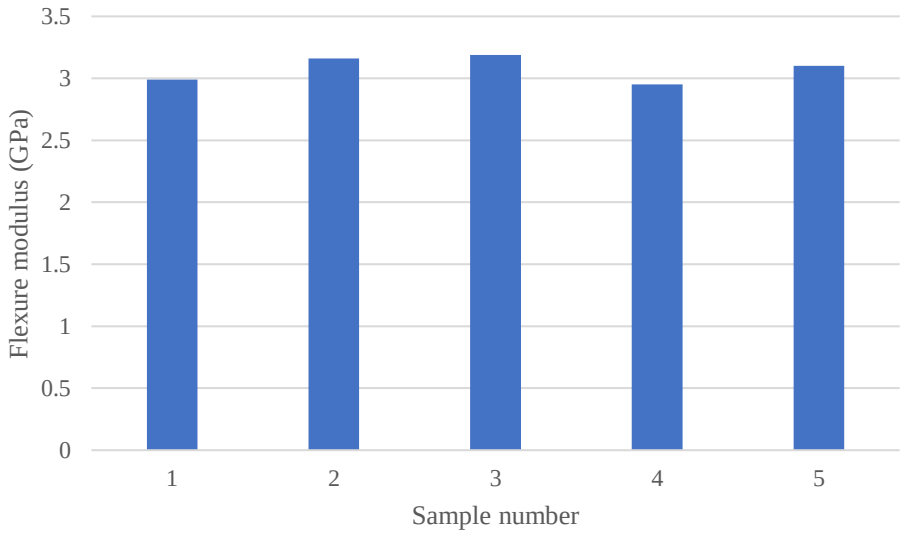

Figure A.24: Flexure modulus of resin and 15% by volume glass fibers.

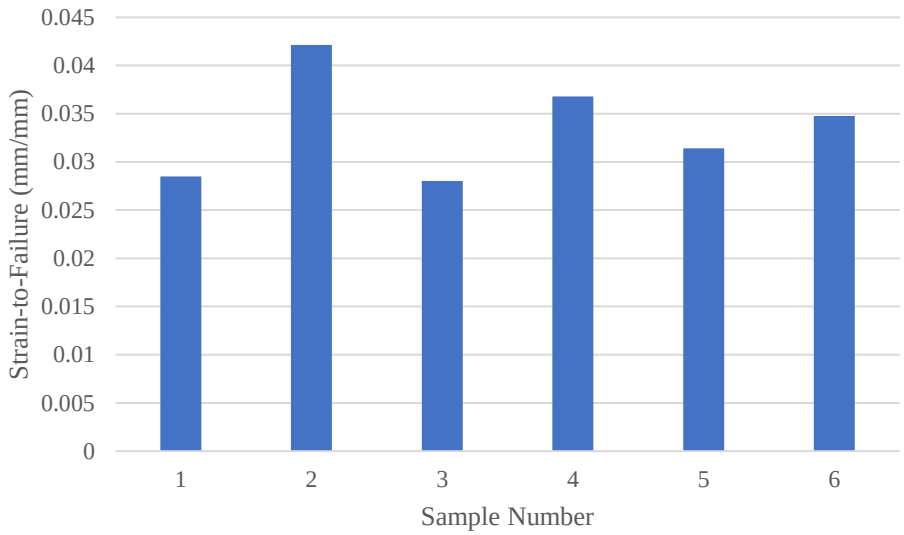

Figure A.25: Strain-to-failure of neat resin samples.

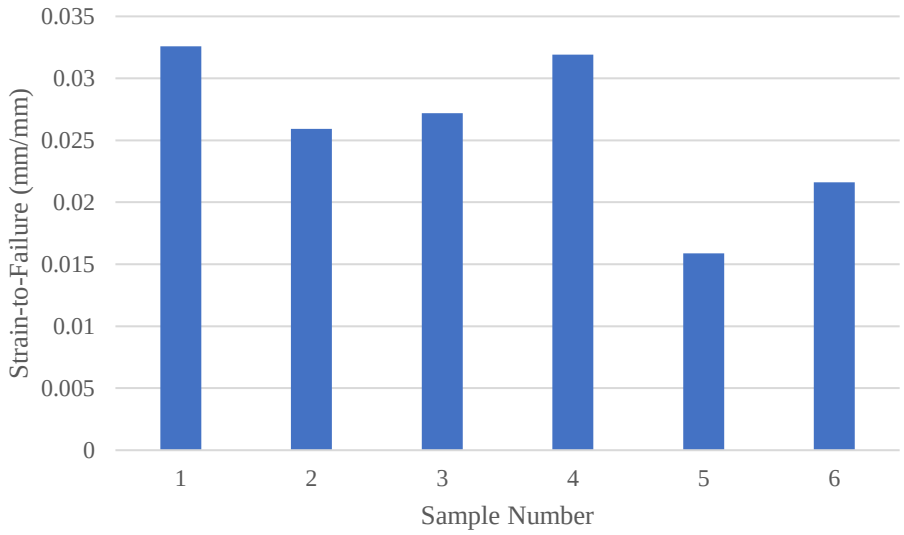

Figure A.26: Strain-to-failure of 15% glass fiber reinforced resin in print orientation PF.

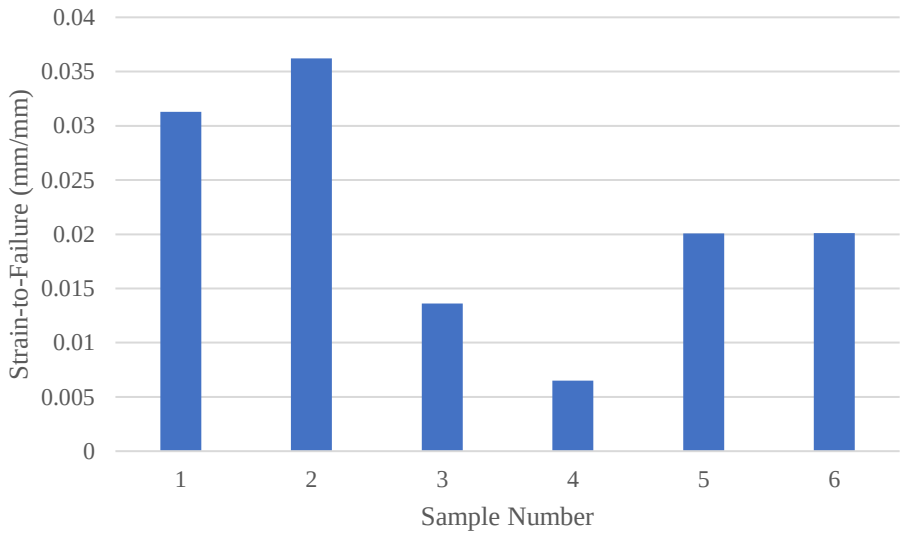

Figure A.27: Strain-to-failure of 15% glass fiber reinforced resin in print orientation TF.

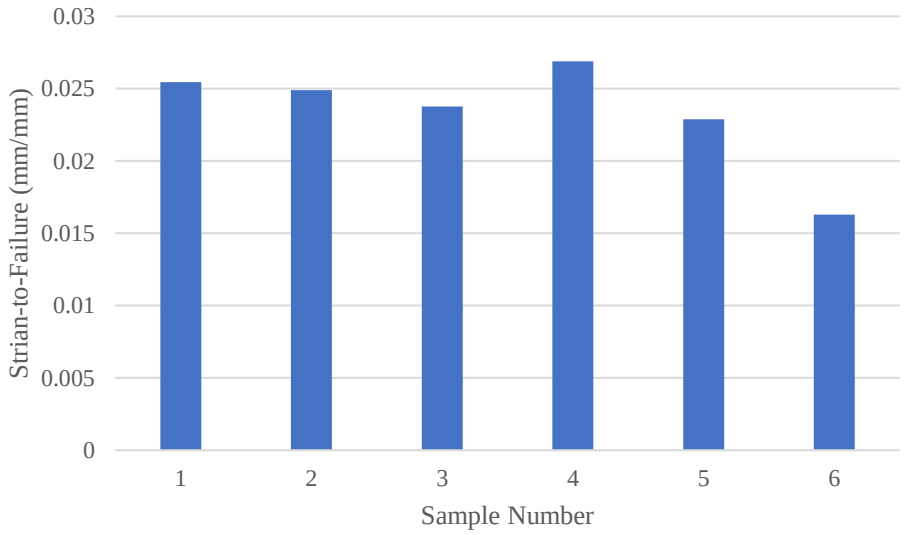

Figure A.28: Strain-to-failure of 15% glass fiber reinforced resin in print orientation TFW.

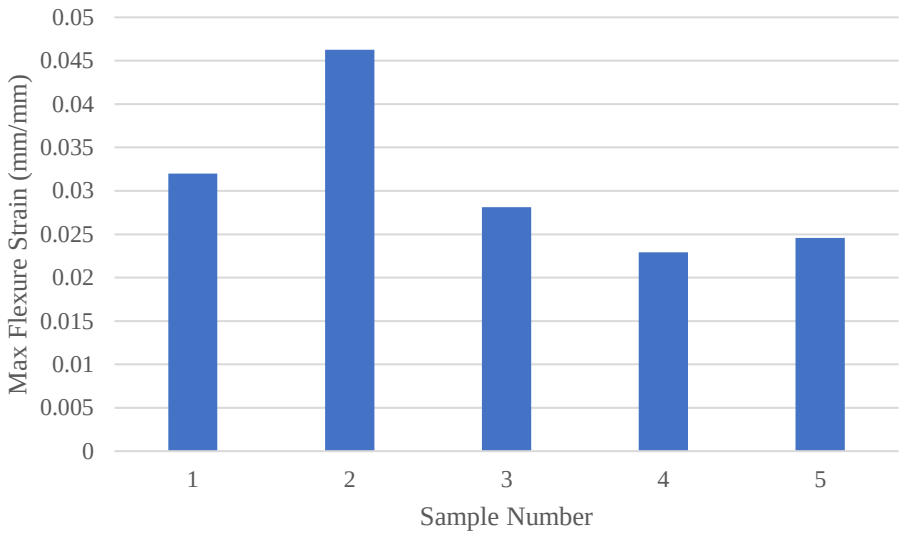

Figure A.29: Max flexure strain of neat samples.

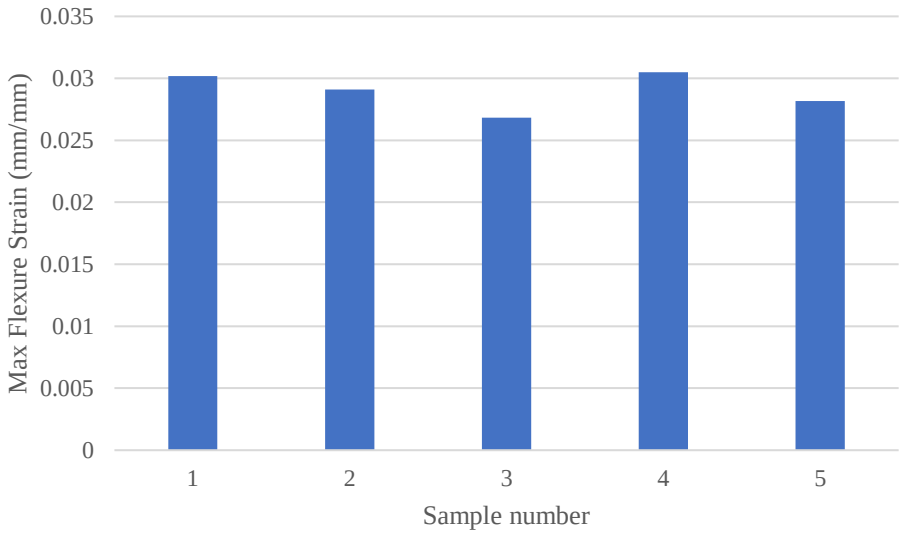

Figure A.30: Max flexure strain of glass fiber reinforced samples.

```
clc
close all
clear all

% Youngs Modulus
EM = 1.6 ; % Matrix (GPa)
EF = 85 ; % Fiber (GPa)

pf = 2.67 ;% Fiber Density (g/cm^3)
pm = 1.0835 ;% Matrix Density (g/cm^3)
% Poisson's
vM = 0.37 ; % Matrix
vF = 0.22 ; % Fiber

V = 0.15; % Fiber Volume
l = 0.00023 ; % Fiber Length (m)
d = 1.6e-5 ; % Fiber Diameter (m)



pc = pf*V + pm*(1-V)
W = (pf/pc) * V ; % Weight Percent of Fiber

Vt = V*100;
Wt = W*100;

disp(['Fiber Volume Percent ',num2str(Vt),])
disp(' ')
disp(['Fiber Weight Percent ',num2str(Wt),])
disp(' ')
disp(['Fiber Length ',num2str(l),])
disp(' ')
disp(['Fiber Diameter ',num2str(d),])
disp(' ')
```

Figure A.31: MatLab code to determine fiber volume and weight.

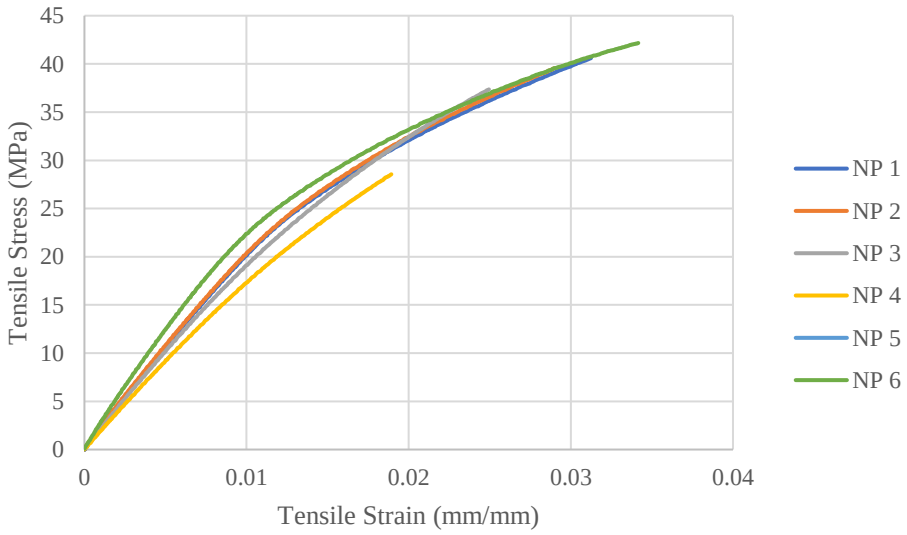

Figure A.32: Stress vs. strain curves of neat samples.

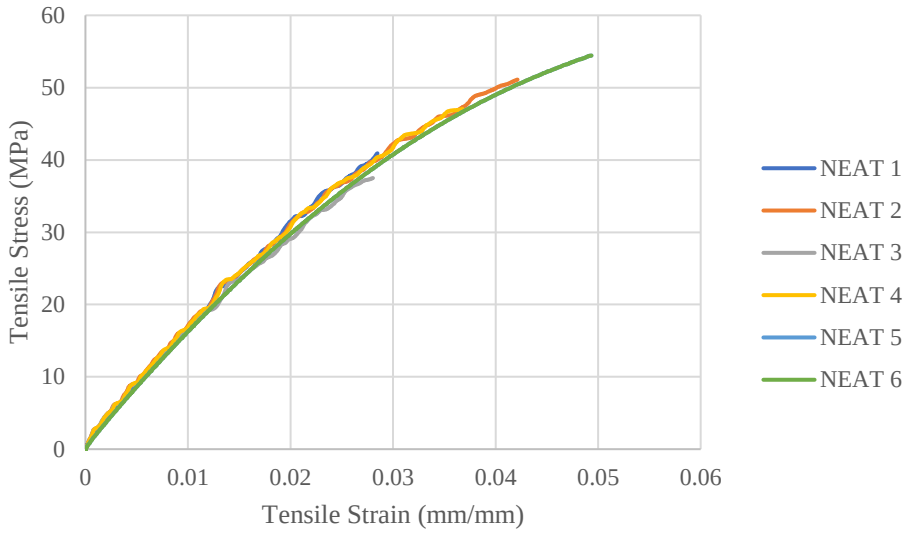

Figure A.33: Stress vs. strain curve of samples with glass fibers but not pump system.

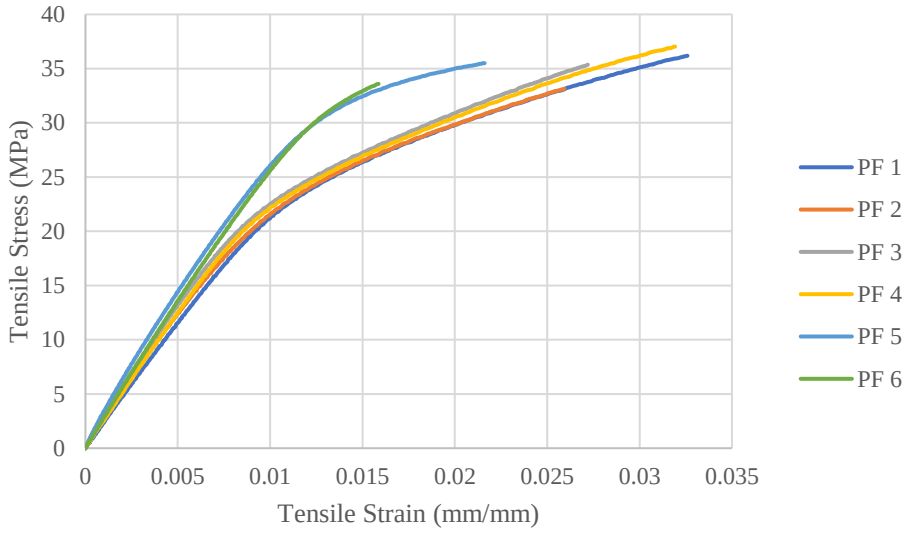

Figure A.34: Stress vs. strain curve of samples printed in the PF orientation with pumping system.

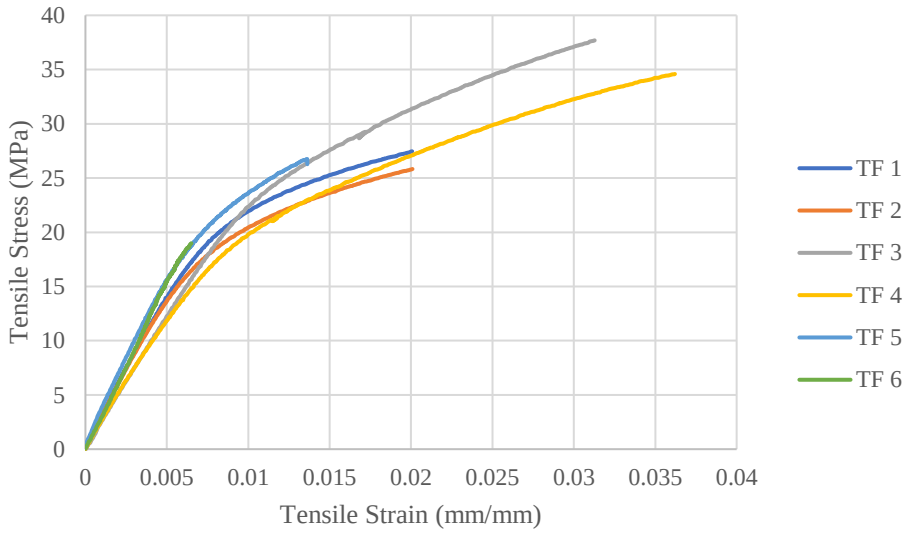

Figure A.35: Stress vs. strain curve of samples printed in the TF orientation with pumping system.

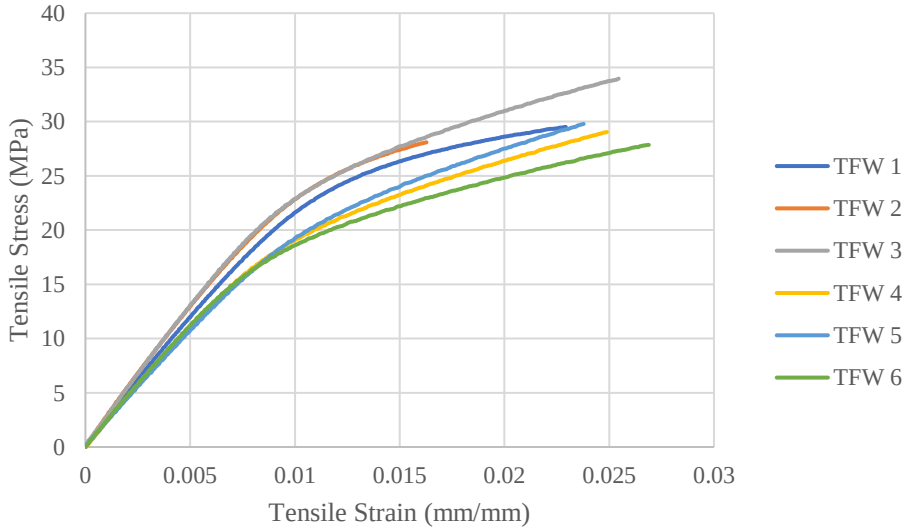

Figure A.36: Stress vs. strain curve of samples printed in the TFW orientation with pumping system.

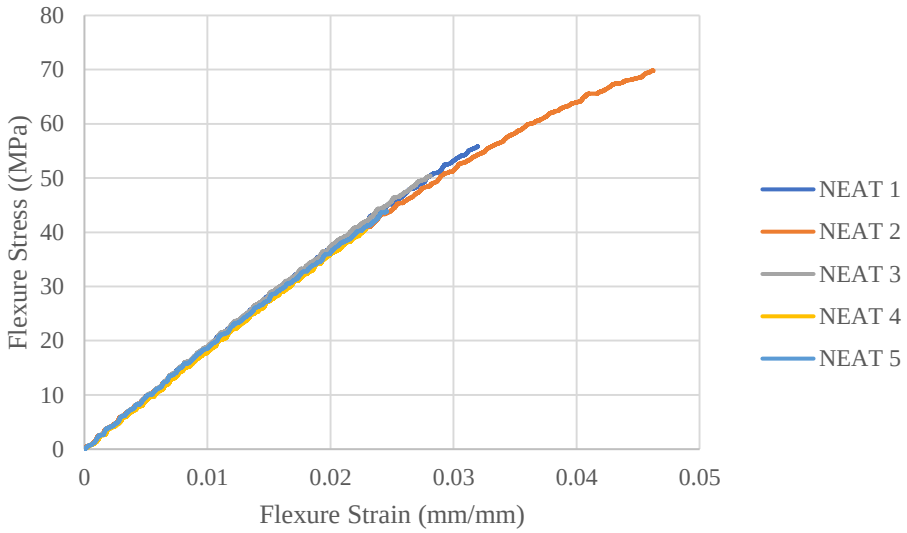

Figure A.37: Stress vs. strain curve of neat flexure samples.

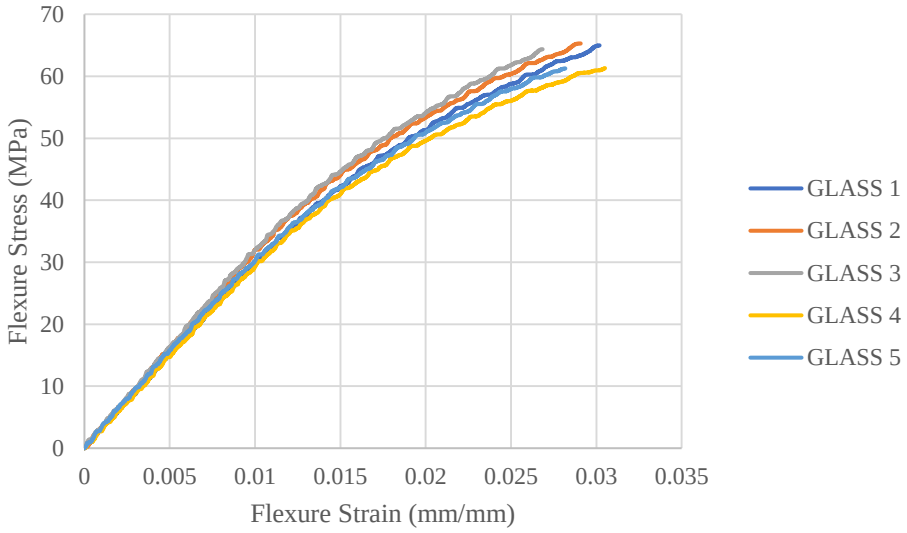

Figure A.38: Stress vs. strain curve of glass fiber reinforced flexure samples.

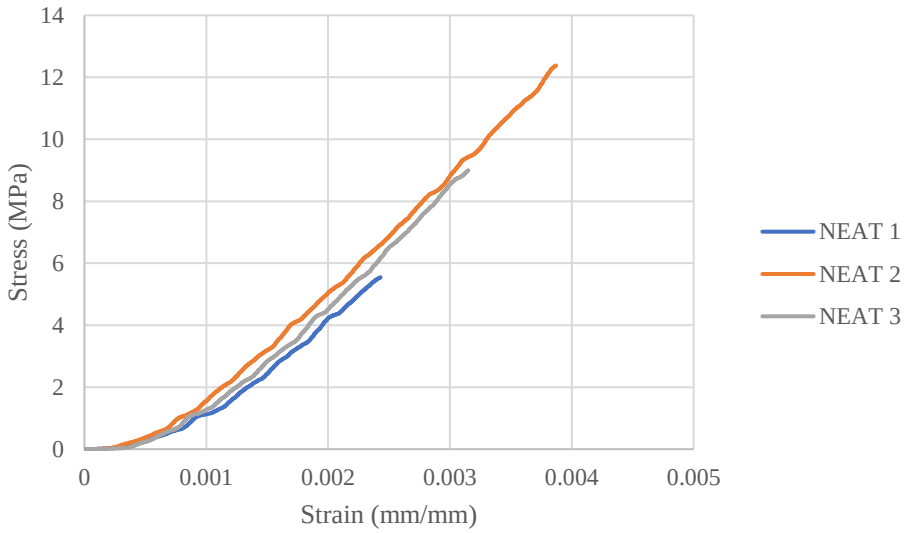

Figure A.39: Stress vs. strain curve of neat notched samples.

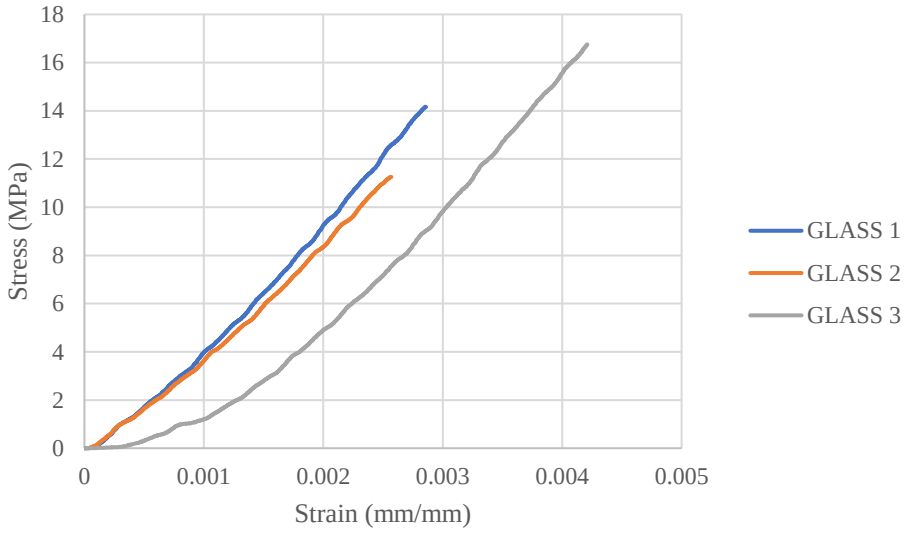

Figure A.40: Stress vs. strain curve of glass reinforced notched samples.